

Numerical Solution Methods for
Control Volume Explosions and ZND Detonation Structure

S. Kao and J. E. Shepherd
Aeronautics and Mechanical Engineering
California Institute of Technology
Pasadena, CA USA 91125

GALCIT Report FM2006.007
July 2004-Revised September 23, 2008

Abstract

Selected algorithms are described for the numerical solution of the governing equations for the constant volume explosion model and the ZND detonation model. In the implementations of these algorithms, we have used the Cantera software library to evaluate gas properties and carry out chemical equilibrium computations. A library of routines is described for Python or Matlab computations which are compatible with methods described in [Browne et al. \(2007\)](#).

Disclaimer and Copyright The software tools described in this document are based on the Cantera software library and offered under the same licensing terms, which are as follows:

Copyright (c) 2001-2007, California Institute of Technology All rights reserved.

Redistribution and use in source and binary forms, with or without modification, are permitted provided that the following conditions are met:

- Redistributions of source code must retain the above copyright notice, this list of conditions and the following disclaimer.

- Redistributions in binary form must reproduce the above copyright notice, this list of conditions and the following disclaimer in the documentation and/or other materials provided with the distribution.

- Neither the name of the California Institute of Technology nor the names of its contributors may be used to endorse or promote products derived from this software without specific prior written permission.

THIS SOFTWARE IS PROVIDED BY THE COPYRIGHT HOLDERS AND CONTRIBUTORS "AS IS" AND ANY EXPRESS OR IMPLIED WARRANTIES, INCLUDING, BUT NOT LIMITED TO, THE IMPLIED WARRANTIES OF MERCHANTABILITY AND FITNESS FOR A PARTICULAR PURPOSE ARE DISCLAIMED. IN NO EVENT SHALL THE COPYRIGHT OWNER OR CONTRIBUTORS BE LIABLE FOR ANY DIRECT, INDIRECT, INCIDENTAL, SPECIAL, EXEMPLARY, OR CONSEQUENTIAL DAMAGES (INCLUDING, BUT NOT LIMITED TO, PROCUREMENT OF SUBSTITUTE GOODS OR SERVICES; LOSS OF USE, DATA, OR PROFITS; OR BUSINESS INTERRUPTION) HOWEVER CAUSED AND ON ANY THEORY OF LIABILITY, WHETHER IN CONTRACT, STRICT LIABILITY, OR TORT (INCLUDING NEGLIGENCE OR OTHERWISE) ARISING IN ANY WAY OUT OF THE USE OF THIS SOFTWARE, EVEN IF ADVISED OF THE POSSIBILITY OF SUCH DAMAGE.

Contents

1	Introduction	9
2	Kinetics Models	9
3	Physical Constraints	12
3.1	Shock Jump Conditions	12
3.2	Equations of Motion	12
3.3	Thermicity	16
3.4	Wave-Fixed Frame	17
4	ZND Detonation Model	18
4.1	Physical Model	18
4.2	Mathematical Model	20
4.2.1	Algebraic Differential System	20
4.2.2	Differential System	22
4.2.3	Length Scales	23
4.2.4	Particle Paths	23
4.3	Eigenvalue Detonation	25
4.4	Numerical Methods	25
4.4.1	Initial Conditions	25
4.4.2	Algorithm	26
4.5	Examples	27
4.5.1	CJ Detonation	27
4.5.2	Overdriven Detonation	29
5	Extensions to the ZND model	31
5.1	Unsteady Model	31
5.2	Steady Curved Wave Model	31
5.3	Steady Detonation with Friction	32
6	Constant Volume Explosion Model	32
6.1	Physical Model	32
6.2	Mathematical Model	33
6.2.1	Algebraic Differential System	33
6.2.2	Differential System	33
6.2.3	Time Scales	34
6.3	Numerical Method	34
6.3.1	Initial Conditions	34
6.3.2	Algorithm	35
6.4	Example	35
7	Constant Pressure Explosion Model	38
7.1	Physical Model	38
7.2	Mathematical Model	38
7.2.1	Algebraic Differential System	38
7.2.2	Differential System	39
7.3	Numerical Method	39
7.4	Example	39

8	Applications	39
8.1	Time Scale Comparison	40
8.2	Effective Activation Energy	40
8.3	Variance with Initial Conditions	40
8.4	Dynamic Detonation Parameters	40
9	Summary	40
A	Temperature Derivatives	43
A.1	Limiting Behavior	44
B	Functions	45
B.1	Constant Volume Explosion	45
B.2	ZND Detonation	45
B.2.1	Matlab Implementation	45
B.2.2	Python/C++ Implementation	46

List of Figures

1	Example of thermicity history for a CJ detonation in a stoichiometric hydrogen-air mixture initially at 300 K and 1 bar.	17
2	Cartoon of the ZND detonation model. (a) States 1, 2, and 3 (b) Reaction zone structure.	19
3	Path (red) between frozen Hugoniot (solid) and equilibrium Hugoniot (dashed) for a ZND detonation traveling at the Chapman-Jouget detonation velocity.	20
4	Space-time diagrams for a CJ detonation (see Browne et al. (2007)) in stoichiometric hydrogen-air. The indicated length scales are the induction length $\Delta_i = 0.160$ mm, the exothermic pulse width $\Delta_e = 0.043$ mm, and the length to an almost equilibrium Mach number ($M = 0.73$) $\Delta_M = 0.462$ mm. The indicated time scales are the induction time $\tau_i = 0.427$ μ s, the exothermic pulse time $\tau_e = 0.087$ μ s, and the time to reach an almost equilibrium Mach number ($M = 0.73$) $\tau_M = 0.847$ μ s. (a) and (b) show the moving shock frame. (c) shows the wave fixed frame.	21
5	Definition of the induction length Δ_i and energy pulse width Δ_e in terms of the thermicity for a CJ detonation in stoichiometric hydrogen-air initially at 300 K and 1 atm. In this case $\Delta_i = 161$ μ m and $\Delta_e = 43$ μ m	24
6	ZND detonation temperature profile simulated by our implementation superimposed over ZND detonation temperature profile simulated by Shepherd's ZND program. The case is hydrogen air with an equivalence ratio of 0.5, an initial temperature of 300 K, an initial pressure of 1 atm, and a shock speed of 2000 m/s.	26
7	ZND structure for a CJ detonation stoichiometric hydrogen-air initially at 300 K and 1 atm. (a) temperature and pressure profiles, (b) density and velocity profiles	27
8	ZND structure for a CJ detonation stoichiometric hydrogen-air initially at 300 K and 1 atm. (a) major species profiles, (b) minor species profiles	28
9	Thermicity ($\dot{\sigma}$) and temperature ZND structure for a CJ detonation in stoichiometric hydrogen-air initially at 300 K and 1 atm.	28
10	Path (red) between frozen Hugoniot (solid) and equilibrium Hugoniot (dashed) for a ZND detonation traveling at $U = 1.1U_{CJ}$	29
11	ZND structure for an overdriven detonation ($U = 1.1U_{CJ}$) stoichiometric hydrogen-air initially at 300 K and 1 atm. (a) temperature and pressure profiles, (b) density and velocity profiles	29
12	ZND structure for an overdriven detonation ($U = 1.1U_{CJ}$) stoichiometric hydrogen-air initially at 300 K and 1 atm. (a) major species profiles, (b) minor species profiles	30
13	Thermicity ($\dot{\sigma}$) and temperature ZND structure for an overdriven detonation ($U = 1.1U_{CJ}$) stoichiometric hydrogen-air initially at 300 K and 1 atm.	30
14	Path (blue) between frozen Hugoniot (solid) and equilibrium Hugoniot (dashed) for a constant volume explosion.	32
15	Definition of the induction time τ_i in terms of the temperature gradient for a constant volume explosion in stoichiometric hydrogen-air initially at the von Neumann point. In this case $\tau_i = 161$ μ s.	34
16	Control volume explosion simulated by PostShock.fr superimposed over control volume explosion simulated by Shepherd's CV program. The case is hydrogen air with an equivalence ratio of 0.5, an initial temperature of 300 K, an initial pressure of 1 atm, and a shock speed of 2000 m/s.	36
17	CV structure for a stoichiometric mixture of hydrogen-air initially at the von Neumann point. (a) temperature and pressure profiles, (b) density and velocity profiles	36
18	CV structure for a stoichiometric mixture of hydrogen-air initially at the von Neumann point. (a) major species profiles, (b) minor species profiles	37
19	Temperature gradient and temperature CV structure for a stoichiometric mixture of hydrogen-air initially at the von Neumann point.	37

20	Path (red) between frozen Hugoniot (solid) and equilibrium Hugoniot (dashed) for a constant pressure explosion.	38
----	---	----

List of Tables

1	Partial hydrogen oxidation mechanism and rate constants (Smith et al., 1999).	11
---	---	----

1 Introduction

A reaction zone model requires two ingredients: a chemistry model and physical constraints. The chemistry model is necessary for conserving species, i.e.

$$\frac{DY_i}{Dt} = \dot{\Omega}_i. \quad (1)$$

while varying the composition through the reaction zone. The constraints assure that the model satisfies conservation of mass, momentum, and energy. Depending on the desired solution technique, these constraints can be expressed algebraically or differentially.

In this report, we present three reaction zone models, the ZND detonation model, the constant volume explosion model, and the constant pressure explosion model. In the ZND detonation model, the reaction zone has a finite length where as in the constant volume model, the reaction happens infinitely fast and in the constant pressure model, the reaction happens infinitely slowly. Each of these models is an approximation of a realistic physical process and offers insight into the structure of the reaction zone.

HISTORY OF THESE MODELS

In Section 2, we describe several different types of chemistry models. Then we present the constraints required for each reaction zone model both algebraically and differentially. Section 4 describes the ZND detonation model, Section 6 describes the constant volume explosion model, and Section 7 describes the constant pressure explosion model. In each of these main sections, there are three subsections. Sections 4.1, 4.2, 6.1, 6.2, 7.1, and 7.2 give physical and mathematical descriptions of each model, Sections 4.4, 6.3 and 7.3 explain the numerical methods, and Sections 4.5, 6.4, and 7.4 provide examples and comparison between results obtained with the Matlab implementation and with legacy Fortran programs (Shepherd, 1986) that we have previously used in our laboratory. Finally, Section 9 summarizes the report.

2 Kinetics Models

All of the implementations included with the Shock and Detonation Toolbox use the ideal gas equation of state.

$$P = \rho RT \quad e = \sum_{i=1}^{N_Y} Y_i e_i(T) \quad h = \sum_{i=1}^{N_Y} Y_i h_i(T) \quad (2)$$

where R is the gas constant for the mixture, T is the temperature, e is the specific internal energy, h is the specific enthalpy, and N_Y is the number of species. An important extension of the ideal gas equation of state is the perfect gas equation of state where the specific heats (c_v, c_p) and their ratio γ are constant. In the perfect gas model, if there is a single progress variable λ ,

$$h = \frac{\gamma}{\gamma - 1} \frac{P}{\rho} - \lambda q \quad (3)$$

where q is the total heat release. In addition to an equation of state we need a kinetics model describing how the composition shifts.

The most realistic set of kinetics models are detailed chemical mechanisms. These models include experimentally validated thermodynamic, transport, and kinetic data. Most commonly, these mechanisms are used within the framework of a thermo-kinetics software package such as CHEMKIN (Kee et al., 1987) or Cantera (Goodwin, 2005). The benefit of detailed mechanisms is that they are intended to represent all chemical aspects of a true system. To this end, the GRI mechanism for methane combustion (Smith et al., 1999) contains 53 species and 285 elementary reactions. Each species is modeled

as an ideal gas with temperature-dependent specific heat, i.e.

$$\left(\frac{c_P}{R}\right)_{\text{H}_2} = \begin{cases} \sum_{k=0}^4 a_k T^k & 200 \text{ K} < T < 1000 \text{ K} \\ \sum_{k=0}^4 b_k T^k & 1000 \text{ K} < T < 6000 \text{ K} \end{cases} \quad (4)$$

where c_P is the specific heat at constant pressure and

$$\{a\}_{\text{H}_2} = \{2.34, 7.98 \cdot 10^{-3}, -1.95 \cdot 10^{-5}, 2.02 \cdot 10^{-8}, -7.38 \cdot 10^{-12}\} \quad (5)$$

$$\{b\}_{\text{H}_2} = \{2.93, 8.27 \cdot 10^{-4}, -1.46 \cdot 10^{-7}, 1.54 \cdot 10^{-11}, -6.89 \cdot 10^{-16}\}. \quad (6)$$

Browne et al. (2007) describes in detail how Cantera uses the above thermodynamic data to compute necessary state properties including h and the specific entropy s .

Additionally, each elementary reaction is reversible with a modified Arrhenius rate coefficient, i.e.,



$$k_f = AT^n \exp\left(\frac{-E_a}{RT}\right) = 1.17000 \cdot 10^9 T^{1.3} \exp\left(\frac{-3626}{RT}\right). \quad (8)$$

where k_f and k_r are the forward and reverse reaction rates, A is the pre-exponential constant, n is the temperature power, and E_a is the activation energy. Because detailed mechanisms model elementary reactions, each reaction is reversible. We use the principle of detailed balance to determine the reverse reaction rate from the forward reaction rate and equilibrium constant.

$$k_r = \frac{k_f}{K_C(T)} \quad (9)$$

where

$$K_C = K_P \left(\frac{P_o}{\mathcal{R}T}\right)^{\Delta\nu}. \quad (10)$$

The condition for chemical equilibrium of the reaction

$$\sum_{i \text{ (sp)}} \nu_i \mu_i = 0 \quad (11)$$

defines K_P , such that

$$K_P = \prod_{i \text{ (sp)}} P_i^{\nu_i} = \exp\left(-\frac{\nu_i [h_i(T) - Ts_i^\circ(T)]}{RT}\right). \quad (12)$$

Here ν is a stoichiometric coefficient, P is pressure, and \mathcal{R} is the ideal gas constant.

Most hydrocarbon mechanisms are built on the the hydrogen mechanism because once the fuel is broken down to radicals, hydrogen chemistry becomes important. The hydrogen mechanism contains 12 species: 3 reactants (H_2 , O_2 , N_2), 1 product (H_2O), 4 radicals (H , O , OH , N), 3 intermediates (HO_2 , H_2O_2 , NO), and 1 inert (Ar). It also contains 24 reactions, and Table 1 shows a selection of these reactions and their rate parameters. There are four primary reaction types in a branching chain: chain initiation, chain branching, chain propagation, and chain termination. In the hydrogen mechanism (Table 1), reaction 1 (backwards) is the initiation reaction. Here the hydrogen molecule reacts with another molecule to produce two hydrogen radicals. Once sufficient free radicals exist, chain branching (Reactions 2–4) and chain propagating reactions (Reaction 5) continue the chain. In each of

No.	Reaction	A	n	E_a
1	$\text{H} + \text{H} + \text{M} \leftrightarrow \text{H}_2 + \text{M}$	$1.00 \cdot 10^{18}$	-1.00	0
2	$\text{O} + \text{OH} \leftrightarrow \text{O}_2 + \text{H}$	$4.00 \cdot 10^{14}$	-0.50	0
3	$\text{O} + \text{H}_2 \leftrightarrow \text{OH} + \text{H}$	$5.06 \cdot 10^4$	2.67	6290.0
4	$\text{OH} + \text{OH} \leftrightarrow \text{O} + \text{H}_2\text{O}$	$6.00 \cdot 10^8$	1.30	0
5	$\text{OH} + \text{H}_2 \leftrightarrow \text{H}_2\text{O} + \text{H}$	$1.17 \cdot 10^9$	1.30	3626.0
6	$\text{H} + \text{O}_2 + \text{M} \leftrightarrow \text{HO}_2 + \text{M}$	$3.61 \cdot 10^{17}$	-0.72	0

Table 1: Partial hydrogen oxidation mechanism and rate constants (Smith et al., 1999).

the branching reactions, two radicals are produced for each radical that reacts. The final process is chain termination which occurs when one or more radicals react to form a stable species. Reaction 6 of the hydrogen mechanism is a termination reaction. Unlike reaction 1, the extra reactant molecule removes energy from the collision between H and O_2 and allows them to bond and form HO_2 .

On the other end of the spectrum is the one-step irreversible model.

$$\mathcal{A} \xrightarrow{k_f} \mathcal{B} \quad (13)$$

$$k_f = A \exp\left(\frac{-E_a}{RT}\right) \quad (14)$$

In this model, there is one irreversible reaction that transforms reactants \mathcal{A} to products \mathcal{B} . The simplest implementations of this model assume that both species have identical and constant specific heat and molecular weights but different heats of formation. The reaction rate coefficient k_f has an Arrhenius form. Although this model is convenient to implement numerically, it is difficult to relate to realistic systems because it only has one time scale and the following four parameters γ , E_a , Δh , A .

Both detailed chemical models and one-step models have limitations: detailed chemical mechanisms are computationally expensive and one-step models are unrealistic. Because of this, several types of reduced models have been investigated. The origins of all simplified models of combustion reactions for explosions can be traced back to the pioneering studies of Semenov (1935) who discovered the key roles of thermal feedback and branching chain reactions in explosions and proposed separate models of each process. A unified model was developed by Gray and Yang (1965) to treat explosions due to simultaneous thermal and chain mechanisms. Since then, researchers have developed two main methods of reducing detailed mechanisms: “timescale separation” methods and pseudo-species methods.

“Timescale separation” methods rely on ordering the many chemical timescales. Tomlin et al. (1997) and Eckett (2000) give reviews of this type of method. Eckett (2000) discusses the QSSA (Quasi-Steady-State Approximation, Peters (1988)) and ILDM (Intrinsic Low Density Manifold, Maas and Pope (1992)) methods extensively. In both of these methods, the chemical timescales are compared with the fluid mechanics timescale and separated into two categories. The reactions that proceed more slowly than the fluid mechanics are modeled with detailed chemistry, while a different model is proposed for those proceeding more quickly than the fluid mechanics. Varatharajan and Williams (2001) and more recently Varatharajan et al. (2005) have also presented work using reduced mechanisms. Like the QSSA and ILDM methods, they used detailed kinetics to model slow timescales and a simplified model to capture the fast timescales.

The second method of reduction is of a more ad hoc nature that addresses the underlying primary chemical pathways. These simple models are in some sense an elaboration of the one-step model, using a notional reaction scheme with multiple steps between a set of pseudo-species in order to mimic the chemical processes. These pseudo-species mechanisms include initiation, branching, and termination steps and are designed to imitate the key features of a realistic chemical reaction mechanism without the computational expense associated with time integration of a large set of species. The two-step model (Korobeinikov et al., 1972) includes an induction region and an energy release region. Oran et al. (1981) improved upon this model by using detailed mechanisms to choose appropriate values for

the induction length and maximum energy release parameters. [Lefebvre et al. \(1992\)](#) further improved the model by allowing the species specific heats and the average molecular weight to be functions of temperature. This generalized the model's original perfect gas equation of state.

3 Physical Constraints

In addition to a kinetics model, a set of physical constraints is also required to completely specify the reaction zone model. The shock jump conditions and the reactive Euler equations are the basis of the physical constraints for the three reaction zone models that we will discuss in this paper. In this section, we will discuss the different forms of these equations and their value. We will recall the *wave-fixed* frame of reference introduced in [Browne et al. \(2007\)](#) and transform the reactive Euler equations to this frame.

3.1 Shock Jump Conditions

The shock jump conditions were described in [Browne et al. \(2007\)](#), but it is useful to clarify their value in reaction zone models. As discussed in [Browne et al.](#), it is most useful to present the jump conditions in the *wave-fixed* frame. In this frame, the steady planar shock is located at a fixed location. The jump conditions are

$$\begin{aligned}\rho w &= \text{constant} \\ P + \rho w^2 &= \text{constant} \\ h + \frac{w^2}{2} &= \text{constant}\end{aligned}\tag{15}$$

where ρ is the density, P is the pressure, h is the specific enthalpy, and w is the normal velocity in the wave-fixed frame. The relationship between w and the lab frame velocity u is

$$w = U_S - u\tag{16}$$

where U_S is the speed of the shock or more generally, the speed of constantly traveling reference point in the frame. We can also combine the jump conditions to form the equation for the Rayleigh line and the Hugoniot curve.

$$\frac{\Delta P}{\Delta v} = - \left(\frac{w_1}{v_1} \right)^2\tag{17}$$

$$\Delta e = \Delta v \frac{P_1 + P_2}{2} \quad \text{or} \quad \Delta h = \Delta P \frac{v_1 + v_2}{2}\tag{18}$$

where $v = 1/\rho$ is the specific volume.

The value of the shock jump conditions is to relate thermodynamic states. An important note is that the jump conditions give no information about the path between states. In the following reaction zone models, we integrate the species conservation equation (Eq. 1) and then use the jump conditions to determine the thermodynamic state at each integration step.

3.2 Equations of Motion

The equations of inviscid motion of a real fluid are the so-called reactive Euler equations, which are simply the conservation of mass, momentum, energy, and species. Both the Lagrangian and Eulerian descriptions of the flow field will be important for deriving the following models. In the Lagrangian description, we focus on the time evolution of a particle (or small control volume), and the material derivative is

$$\frac{D}{Dt} = \frac{d}{dt} \Big|_{X_p}\tag{19}$$

where X_p is the particle path. On the other hand, in the Eulerian description, we focus on a control volume with material flowing in and out. In this case, the fields (i.e. ρ , P , \mathbf{u}) can vary with time and space, and in the wave-fixed frame, the material derivative is

$$\frac{D}{Dt} = \frac{\partial}{\partial t} + \mathbf{u} \cdot \nabla. \quad (20)$$

Therefore the two descriptions are related by

$$\left. \frac{d}{dt} \right|_{X_p} = \frac{\partial}{\partial t} + \mathbf{u} \cdot \nabla. \quad (21)$$

We will derive the necessary equations of motion with the Eulerian description and use Eq. 21 to transform to the Lagrangian description when needed.

In a fixed (inertial) reference frame, the reactive Euler equations are:

$$\frac{D\rho}{Dt} = -\rho \nabla \cdot \mathbf{u} \quad (22)$$

$$\rho \frac{D\mathbf{u}}{Dt} = -\nabla P \quad (23)$$

$$\rho \frac{D}{Dt} \left(h + \frac{|\mathbf{u}|^2}{2} \right) = \frac{\partial P}{\partial t} \quad (24)$$

$$\frac{DY_i}{Dt} = \dot{\Omega}_i \quad (25)$$

By combining the energy equation (Eq. 24) and the momentum equation (Eq. 23), we can also express energy conservation with either of the following equations.

$$\frac{De}{Dt} = \frac{P}{\rho^2} \frac{D\rho}{Dt} \quad (26)$$

$$\frac{Dh}{Dt} = \frac{1}{\rho} \frac{DP}{Dt} \quad (27)$$

Note that the chemistry appears explicitly only in the last term of Eq. 25 and that the first three equations, Eqs. 22-24, apparently do not involve chemical reaction. These first three equations are sufficient for modeling nonreactive flows such as shock waves or even the simple hydrodynamic model of detonations. Apparently the fluid dynamics of detonations and nonreactive shock waves are essentially identical and the influence of chemical reaction is expressed indirectly through the dependence of the enthalpy and pressure functions on the composition. Analyses of shock and detonation waves do have many common elements but the apparent independence of the fluid dynamics from the chemistry is an illusion. An explicit coupling can be demonstrated by examining the problem in other variables.

Entropy Formulation of the Energy Equation

The coupling between chemistry and fluid dynamics can be more explicitly displayed by substituting an evolution equation for specific entropy s or specific enthalpy h . Introduce the *fundamental property relation of thermodynamics* for a fixed mass of material:

$$dh = Tds + \frac{dP}{\rho} + \sum_{i=1}^{N_Y} g_i dY_i \quad (28)$$

where g_i is the specific Gibbs energy of species i . The changes dh , ds , etc. refer to variations within a certain mass of material or fluid element. These changes are identical to those associated with the material derivative. With this correspondence $dh \rightarrow Dh/Dt$, etc., we can then combine Eqs. 24, 25, and 28 to obtain an entropy form of the energy equation.

$$\frac{Ds}{Dt} = -\frac{1}{T} \sum_{i=1}^{N_Y} g_i \dot{\Omega}_i. \quad (29)$$

Physically, this relation indicates that the entropy in a smooth, inviscid flow changes only due to chemical reaction. Of course, in a discontinuous flow i.e., one with shocks, there can be jumps in entropy without any chemical reaction. The entropy equation (Eq. 29) has exactly the form of a nonreactive entropy equation in a flow with heat addition, where the equivalent heat addition per unit volume is

$$q = -\rho \sum_{i=1}^{N_Y} g_i \dot{\Omega}_i \quad (30)$$

This correspondence enables many aspects of adiabatic, compressible, and reacting flow to be interpreted in terms of better known results of nonreacting, diabatic, compressible flows. However, one should always keep in mind that the equivalent heat addition is dependent on the flow itself in a complex, nonlinear fashion through the reaction mechanism and rate expressions.

Adiabatic Change Equation

Another form of the energy equations arises when we expand pressure as a function of density, specific entropy, and species, $P(\rho, s, \mathbf{Y})$.

$$dP = \left. \frac{\partial P}{\partial \rho} \right|_{s, \mathbf{Y}} d\rho + \left. \frac{\partial P}{\partial s} \right|_{\rho, \mathbf{Y}} ds + \sum_{i=1}^{N_Y} \left. \frac{\partial P}{\partial Y_i} \right|_{\rho, s, Y_{k \neq i}} dY_i \quad (31)$$

Substitute for ds from Eq. 29 to obtain

$$\frac{DP}{Dt} = \left. \frac{\partial P}{\partial \rho} \right|_{s, \mathbf{Y}} \frac{D\rho}{Dt} + \sum_{i=1}^{N_Y} \left[-\frac{g_i}{T} \left. \frac{\partial P}{\partial s} \right|_{\rho, \mathbf{Y}} + \left. \frac{\partial P}{\partial Y_i} \right|_{\rho, s, Y_{k \neq i}} \right] \frac{DY_i}{Dt} \quad (32)$$

We refer to this as the adiabatic change equation, also discussed by [Fickett and Davis \(1979\)](#).

Sound Speeds

The entropy formulation establishes the connection between chemical reaction and thermodynamic state changes. In nonreactive, adiabatic flows, the equation set (Eqs. 22-24) can be written as

$$\frac{D\rho}{Dt} = -\rho \nabla \cdot \mathbf{u} \quad (33)$$

$$\frac{D\mathbf{u}}{Dt} = -\frac{1}{\rho} \nabla P \quad (34)$$

$$\frac{Ds}{Dt} = 0 \quad (35)$$

This equation set has to be supplemented by a relationship of the form $s(P, \rho)$. Although these equations apparently describe smooth (differentiable) flows, shocks or contact surfaces can exist that must be represented as discontinuities in properties. The equations must be supplemented by the shock jump conditions in those cases.

Considering entropy to be a function of pressure and density $s(P, \rho)$, we obtain

$$ds = \left. \frac{\partial s}{\partial P} \right|_{\rho} dP + \left. \frac{\partial s}{\partial \rho} \right|_P d\rho = 0 \quad \text{or} \quad dP = \left. \frac{\partial P}{\partial \rho} \right|_s d\rho \quad (36)$$

This is more conventionally written as

$$dP = a_f^2 d\rho \quad \text{or} \quad a_f^2 = \left. \frac{\partial P}{\partial \rho} \right|_s \quad (37)$$

where a_f is the sound speed. More precisely, this is the frozen sound speed since the composition is fixed

$$a_f^2 = \left. \frac{\partial P}{\partial \rho} \right|_{s, \mathbf{Y}} \quad (38)$$

One problem that arises in generalizing the isentropic relation, Eq. 38, is the potential difficulty in defining sound speed in a reactive flow. At least two definitions are possible. The equilibrium sound speed

$$a_e^2 = \left. \frac{\partial P}{\partial \rho} \right|_{s, \mathbf{Y}_{eq}} \quad (39)$$

corresponds to velocity of propagation for very slow disturbances in which the fluid composition remains in chemical equilibrium at all times. This is the sound speed used to compute the Mach number on which the CJ condition is conventionally based. The frozen sound speed, Eq. 38, is based on a fixed composition and is appropriate for rapidly traveling disturbances. This is the sound speed that logically appears as a result of the derivations. It is used to define the Mach number used in the reaction zone structure computations and is appropriate for generalizing the isentropic equation.

Under most circumstances the difference between equilibrium and frozen sound speed at the end of the reaction zone is negligible, a few percent at most. However, for mixtures that contain gases of disparate specific heat ratio γ (such as $\text{H}_2\text{-O}_2\text{-Ar}$), the difference may become significant, up to $\approx 10\%$. In an ideal gas, the frozen sound speed can be computed exactly as in a nonreactive flow, $a_f^2 = \gamma RT$.

The real difficulty is that the term *sound speed* is commonly used to denote both a defined quantity (either Eq. 38 or 39) and the physical speed of the propagation of small disturbances. The process of disturbance propagation in reactive flows is considerably more complex than in nonreactive flow and in fact, the notion of a unique sound speed and fixed amplitude disturbances are not applicable. As the brief discussion above indicates, the speed of propagation will depend on frequency of the disturbances, which is the hallmark of a *dispersive* wave and as we will see subsequently, the amplitude of the disturbances will either grow or decay depending on the chemical processes. This gives rise to hierarchies of wave motion which prevent simple interpretation of propagation processes in terms of a single propagation speed.

Now that we have defined the frozen sound speed, Eq. 32 becomes

$$\frac{DP}{Dt} = a_f^2 \frac{D\rho}{Dt} + \sum_{i=1}^{N_Y} \left[-\frac{g_i}{T} \left. \frac{\partial P}{\partial s} \right|_{\rho, \mathbf{Y}} + \left. \frac{\partial P}{\partial Y_i} \right|_{\rho, s, Y_{k \neq i}} \right] \frac{DY_i}{Dt} \quad (40)$$

The bracketed term on the left-hand side has dimensions of a_f^2 so it is convenient to define a quantity thermicity $\dot{\sigma}$ which has dimensions of reciprocal time s^{-1} and write this equation as

$$\frac{DP}{Dt} = a_f^2 \frac{D\rho}{Dt} + \rho a_f^2 \dot{\sigma} \quad (41)$$

3.3 Thermicity

The thermicity term can be broken down into two parts, a dimensionless coefficient σ_i that depends on thermodynamic properties and the convective derivative of the species mass fractions

$$\dot{\sigma} = \sum_{i=1}^{N_Y} \sigma_i \frac{DY_i}{Dt} \quad (42)$$

As written, the coefficients σ_i in the thermicity term are difficult to compute since the necessary partial derivatives are not commonly available for a typical equation of state. Using thermodynamic identities, the following version can be obtained

$$\sigma_i = -\frac{1}{\rho} \left. \frac{\partial \rho}{\partial Y_i} \right|_{P,T,Y_{k \neq i}} - \frac{\alpha_T}{c_P} \left. \frac{\partial h}{\partial Y_i} \right|_{P,T,Y_{k \neq i}} \quad (43)$$

Note that this relation is completely general and is independent of any assumptions about the equation of state or the reaction mechanism. The coefficient of thermal expansion is

$$\alpha_T = -\frac{1}{\rho} \left. \frac{\partial \rho}{\partial T} \right|_{P,\mathbf{Y}} \quad (44)$$

For an ideal gas, further simplification is possible and we find that

$$\sigma_i = \frac{\bar{W}}{W_i} - \frac{h_i}{c_P T} \quad (45)$$

which is straight forward to evaluate from available thermodynamic functions. A simpler derivation of the thermicity function proceeds by considering the enthalpy directly, expanding $h(P, \rho, \mathbf{Y})$ to obtain

$$dh = \left. \frac{\partial h}{\partial P} \right|_{\rho,\mathbf{Y}} dP + \left. \frac{\partial h}{\partial \rho} \right|_{P,\mathbf{Y}} d\rho + \sum_{i=1}^{N_Y} \left. \frac{\partial h}{\partial Y_i} \right|_{P,\rho,Y_{k \neq i}} dY_i \quad (46)$$

and eliminating the enthalpy using Eq. 24 to obtain the following version of the adiabatic change relation

$$\left(1 - \left. \frac{\partial h}{\partial P} \right|_{\rho,\mathbf{Y}} \right) dP = \left. \frac{\partial h}{\partial \rho} \right|_{P,\mathbf{Y}} d\rho + \sum_{i=1}^{N_Y} \left. \frac{\partial h}{\partial Y_i} \right|_{P,\rho,Y_{k \neq i}} dY_i \quad (47)$$

where we have used the identity

$$\left. \frac{\partial h}{\partial Y_i} \right|_{P,\rho,Y_{k \neq i}} = g_i \quad (48)$$

This can be further simplified with the following thermodynamic identities

$$a_f^2 = \frac{\left. \frac{\partial h}{\partial \rho} \right|_{P,\mathbf{Y}}}{\frac{1}{\rho} - \left. \frac{\partial h}{\partial P} \right|_{\rho,\mathbf{Y}}} \quad \left. \frac{\partial h}{\partial \rho} \right|_{P,\mathbf{Y}} = -\frac{c_P}{\rho \alpha_T} \quad (49)$$

which results in the following alternative expression for the thermicity coefficient

$$\sigma_i = -\frac{\alpha_T}{c_P} \left. \frac{\partial h}{\partial Y_i} \right|_{P,\rho,Y_{k \neq i}} \quad (50)$$

The entire coupling between the flow and the chemistry is contained with $\dot{\sigma}$. Thermicity measures the rate at which chemical energy is transformed into thermal energy and vice versa. The variation of the thermicity within the flow reflects the net effect of all chemical reactions taking place: bimolecular exchanges, recombination and dissociation. The magnitude and sign of $\dot{\sigma}$ depends on the rate at which each process is occurring, the net amount of energy released or absorbed, and the net creation or destruction of molecules.

The first term in Eq. 43 is the effective energy release associated with changing the total number of moles of species per unit mass of the reacting mixture. The second term in Eq. 43 is the normalized energy release associated with chemical bond breaking and formation. Normally, the second term completely dominates the first. In those cases, if the dominant processes are endothermic reactions, $\dot{\sigma} < 0$; if the dominant processes are exothermic reactions, $\dot{\sigma} > 0$.

Thermicity is a dynamic property and depends on the evolution of the system. However, for steady detonation, the dependence of the thermicity function on time is straightforward. A typical thermicity history is shown in Fig. 1.

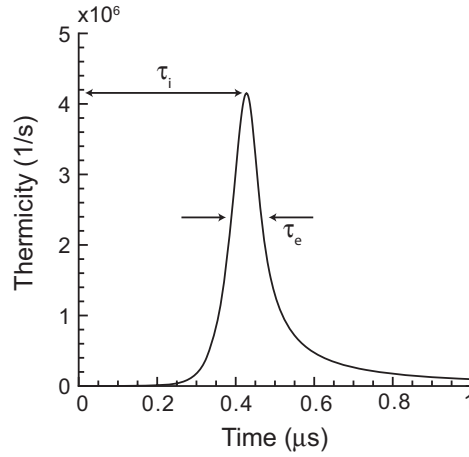


Figure 1: Example of thermicity history for a CJ detonation in a stoichiometric hydrogen-air mixture initially at 300 K and 1 bar.

There are two key features of the thermicity: a) there is dwell or induction time τ_i during which very little energy is released or absorbed; b) there is a single energy release event that occurs over a characteristic time τ_e . The relevance of these time scales is in comparison to the time scale of other flow processes such as flow diffraction time, acoustic wave propagation time and instability period. The simplest notion used in analyzing detonations is that the induction time provides the fundamental time scale that determines the other critical time scales in the problem. While only approximately true, this provides a key link between the chemical processes and the macroscopic wave behavior.

3.4 Wave-Fixed Frame

For future derivation, it is valuable to transform this to the wave-fixed reference frame. We will limit the transformation to a single spatial dimension, but a multi-dimension derivation is similar. In the wave-frame,

$$\begin{aligned} x &= X_S - x^L \\ t &= t^L \\ w &= U_S - u \end{aligned} \tag{51}$$

where X_S is the position of the shock, and the derivatives become

$$\frac{\partial}{\partial x^L} = -\frac{\partial}{\partial x} \quad (52)$$

$$\frac{\partial}{\partial t^L} = \frac{\partial X_S}{\partial t} \frac{\partial}{\partial x} + \frac{\partial}{\partial t} = U_S \frac{\partial}{\partial x} + \frac{\partial}{\partial t}$$

$$\frac{D}{Dt^L} \rightarrow \frac{D}{Dt} = \frac{\partial}{\partial t} + w \frac{\partial}{\partial x} \quad (53)$$

Finally, the one-dimensional reactive Euler equations in the wave-frame are

$$\begin{aligned} \frac{D\rho}{Dt} + \rho \frac{\partial w}{\partial x} &= \rho \frac{\partial U_S}{\partial x} \\ \rho \frac{Dw}{Dt} + \frac{\partial P}{\partial x} &= \rho \frac{DU_S}{Dt} \\ \frac{DP}{Dt} = a_f^2 \frac{D\rho}{Dt} + \rho a_f^2 \dot{\sigma} \quad \text{or} \quad \rho \frac{D}{Dt} \left(h + \frac{w^2}{2} \right) - \frac{\partial P}{\partial t} &= U_S \frac{\partial P}{\partial x} - \rho \frac{D}{Dt} \left[U_S \left(\frac{U_S - 2w}{2} \right) \right] \\ \frac{DY_i}{Dt} &= \dot{\Omega}_i \end{aligned} \quad (54)$$

The adiabatic change equation remains identical in both frames. If the wave speed is constant, the equations reduce further, i.e.

$$\begin{aligned} \frac{D\rho}{Dt} + \rho \frac{\partial w}{\partial x} &= 0 \\ \rho \frac{Dw}{Dt} + \frac{\partial P}{\partial x} &= 0 \\ \frac{DP}{Dt} - a_f^2 \frac{D\rho}{Dt} = \rho a_f^2 \dot{\sigma} \quad \text{or} \quad \rho \frac{D}{Dt} \left(h + \frac{w^2}{2} \right) - \frac{\partial P}{\partial t} &= 0 \\ \frac{DY_i}{Dt} &= \dot{\Omega}_i \end{aligned} \quad (55)$$

In the above derivation, we assumed that, in the wave-fixed frame, there was a shock wave located at X_S . It is important to note that Eq. 55 applies to reference frames moving with a constant velocity. As we will discuss, for the constant volume and constant pressure explosion models, the initial conditions do not need to be shock-heated reactants. In fact, no shock is required for these models, but Eq. 55 still applies.

4 ZND Detonation Model

The ZND detonation model is a one-dimensional steady model, which can be expressed by an algebraic-differential system of equations or a purely differential system of equations. First we will discuss physical and graphical interpretations of this model. Then we will present the algebraic-differential system of equations for this model which are derived from the jump conditions (see discussion in Browne et al. (2007)) followed by two forms of the purely differential system of equations. Finally, we will discuss the eigenvalue detonation.

4.1 Physical Model

A detonation is a supersonic combustion wave in which a shock wave and a reaction zone are coupled. The leading shock raises the temperature and pressure of a mixture of fuel and oxidizer initiating a coupled thermal branching-chain explosion. After an induction time, exothermic recombination reactions create

product species whose expansion acts as a piston propelling the shock wave forward. The interaction between the leading shock and consequent reaction zone is a defining characteristic of self-sustained detonations.

The simplest detonation model, the ZND model, was developed in the 1940s independently by Zel'dovich (1940), von Neumann (1942), and Doering (1943). In this model, shown in the wave-fixed frame in Fig. 2a, a frozen shock is followed by a finite reaction zone. State 1 is a cold mixture of reactants, state 2 is a shocked (hot) mixture of the same reactants, and state 3 is the equilibrium state of the reactive mixture. This model assumes that the composition does not change between states 1 and 2. Within the reaction zone, there are two main length scales: Δ_i , the induction length, and Δ_e , the energy release pulse width. These two scales will be discussed further in relation to the mathematical model. The equations presented in the mathematical model approximate the path between states 2 and 3.

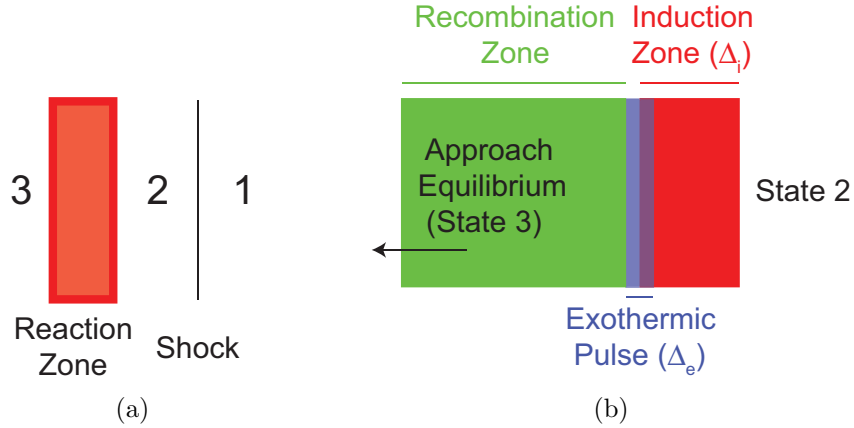


Figure 2: Cartoon of the ZND detonation model. (a) States 1, 2, and 3 (b) Reaction zone structure.

Figure 3 illustrates how we can visualize this model in the P - v plane with the Rayleigh line (Eq. 17) and Hugoniot curve (Eq. 18). A frozen shock wave connects states 1 and 2. We see that in this figure, the Rayleigh line is tangent to the product Hugoniot which indicates that this is the CJ case (Browne et al., 2007, see). State 2, the frozen post-shock state, for the CJ case is often called the von Neumann point. For an overdriven detonation, state 2 is simply the frozen post-shock state. State 3 lies on the same Rayleigh line, but on the equilibrium Hugoniot rather than the frozen Hugoniot. We see that in the ZND model, both the pressure and the specific volume vary through the reaction zone. In reactive systems, there are many Hugoniot curves for each amount of partial reaction ranging from frozen to total equilibrium. Although only the frozen and equilibrium Hugoniots are shown in Fig. 3 each point along the red line connecting states 2 and 3 lies on a partial equilibrium Hugoniot.

A third graphical interpretation of the ZND model is a space-time (x - t) diagram. Figure 4 shows the shock traveling at a constant velocity as well as the induction zone, energy release zone, and Mach number $M = 0.73$ location. In this case, a CJ detonation in stoichiometric hydrogen air, the end of the reaction zone coincides with the sonic plane ($M = 1$). The sonic plane is far from the induction zone and is not shown in Figure 4. A particle path is superposed to indicate how a packet of fluid initially at rest is accelerated through the shock. In the lab frame, Figures 4a and b, the particle decelerates through the reaction zone, and in the wave-fixed frame, Figure 4c, the particle accelerates through the reaction zone. This behavior can be explained by Eq. 16 because in the lab frame, the particle path is defined by

$$\frac{dX_p^L}{dt^L} = u, \quad (56)$$

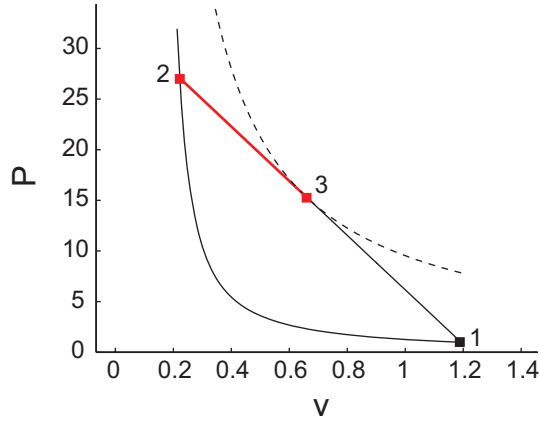


Figure 3: Path (red) between frozen Hugoniot (solid) and equilibrium Hugoniot (dashed) for a ZND detonation traveling at the Chapman-Jouget detonation velocity.

and in the wave-fixed frame, the particle path is

$$\frac{dX_p}{dt} = w. \quad (57)$$

4.2 Mathematical Model

The ZND model is steady meaning that the fields in the Eulerian description are unchanging in time, i.e.

$$\frac{\partial}{\partial t} = 0, \quad (58)$$

which means that Eq. 21 becomes

$$\left. \frac{d}{dt} \right|_{X_p} = w \frac{d}{dx}. \quad (59)$$

4.2.1 Algebraic Differential System

The algebraic-differential system of equations corresponds to the steady conservation of species equation

$$w \frac{dY_i}{dx} = \dot{\Omega}_i \quad (60)$$

and a set of algebraic constraints determined by the shock jump conditions (Eq. 15). In order to specify these algebraic constraints, we assume a reference state $(\cdot)_r$. We start with the conservation of mass and find an expression for the density ρ as a function of the normal velocity u .

$$\rho u = \text{constant} \quad \rightarrow \quad \rho = \frac{(\rho u)_r}{u} \quad (61)$$

Then, using Eq. 61, the conservation of momentum gives an expression for u as a function of P .

$$P + \rho u^2 = \text{constant} \quad \rightarrow \quad u = \frac{P_r - P}{(\rho u)_r} + u_r \quad (62)$$

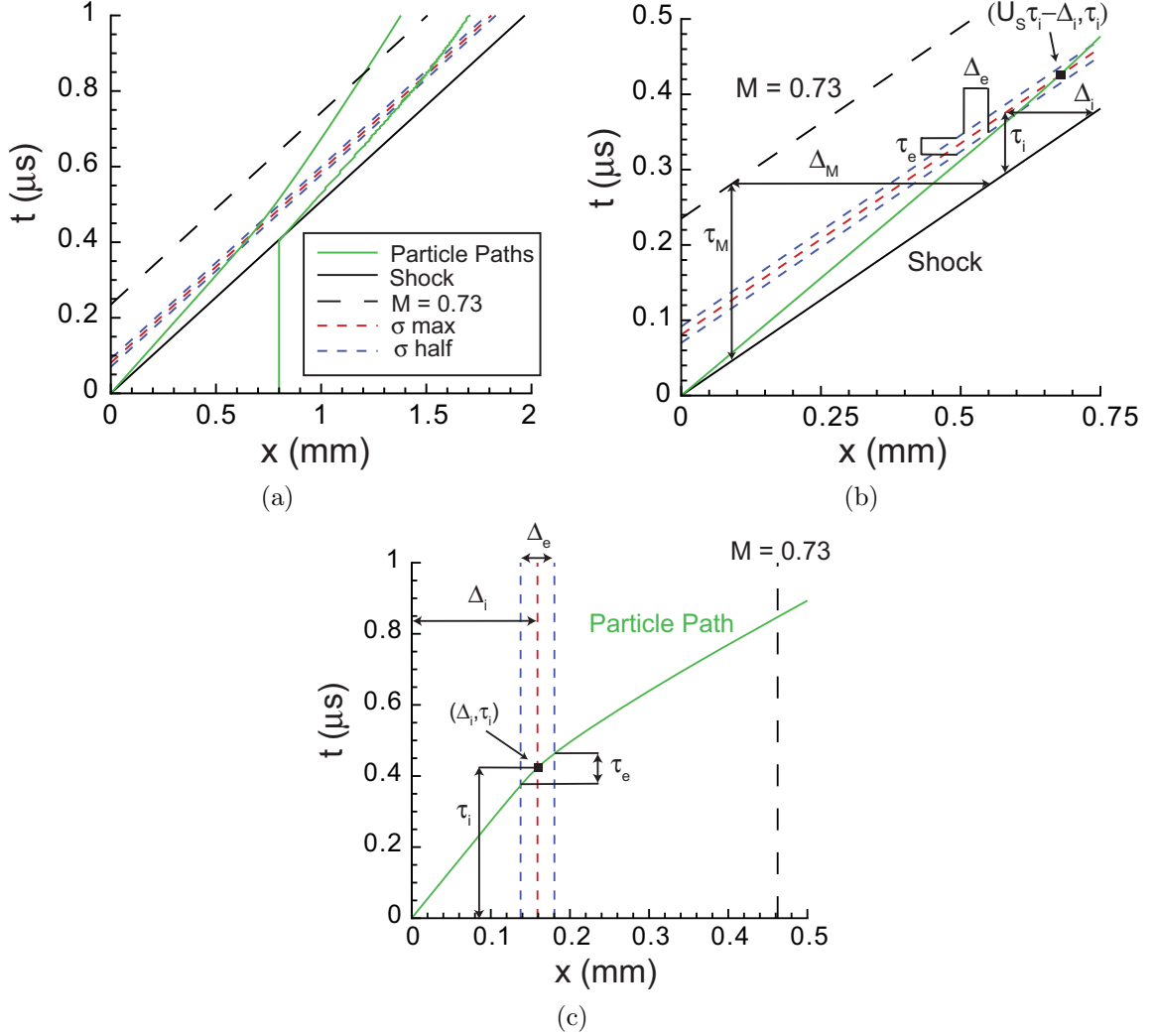


Figure 4: Space-time diagrams for a CJ detonation (see Browne et al. (2007)) in stoichiometric hydrogen-air. The indicated length scales are the induction length $\Delta_i = 0.160$ mm, the exothermic pulse width $\Delta_e = 0.043$ mm, and the length to an almost equilibrium Mach number ($M = 0.73$) $\Delta_M = 0.462$ mm. The indicated time scales are the induction time $\tau_i = 0.427$ μ s, the exothermic pulse time $\tau_e = 0.087$ μ s, and the time to reach an almost equilibrium Mach number ($M = 0.73$) $\tau_M = 0.847$ μ s. (a) and (b) show the moving shock frame. (c) shows the wave fixed frame.

Finally, if we insert Eqs. 61 and 62 into the conservation of energy to find the following expression in terms of P and h .

$$h + \frac{u^2}{2} = \text{constant} \quad \rightarrow \quad h(T) = aP^2 + bP + c \quad (63)$$

$$\begin{aligned} a &= - \left[\frac{1}{\rho u} \right]_r^2 \\ b &= 2 \left[\frac{P - \rho u^2}{(\rho u)^2} \right]_r \\ c &= \left[h(T) + \frac{u}{2} - \frac{(P + \rho u^2)^2}{(\rho u)^2} \right]_r \end{aligned} \quad (64)$$

In the case of a perfect gas ($\gamma = \text{constant}$) with a single progress variable, we can use $h(T)$ (Eq. 3) to specify P in terms of reference quantities.

$$\begin{aligned}
a'P^2 + b'P + c' &= 0 \\
a' &= -\frac{\gamma + 1}{2\gamma(\rho u)_r^2} \\
b' &= \frac{1}{\gamma} \left[\frac{P + \rho u^2}{(\rho u)^2} \right]_r \\
c' &= \frac{1}{2\gamma} \left[\left(\frac{P}{\rho} \right)_r \left[(\gamma - 1) \left(\frac{P}{\rho u^2} \right)_r - 2 \right] - \lambda q \frac{\gamma - 1}{\gamma} \right]
\end{aligned} \tag{65}$$

4.2.2 Differential System

To find the purely differential system of equations, we use the steady form of the one-dimensional reactive Euler equations in the wave-fixed frame (Eq. 55).

$$w \frac{d\rho}{dx} + \rho \frac{dw}{dx} = 0 \tag{66}$$

$$\rho w \frac{dw}{dx} + \frac{dP}{dx} = 0 \tag{67}$$

$$w \left(\frac{dP}{dx} - \frac{d\rho}{dx} \right) = \rho a_f^2 \dot{\sigma} \tag{68}$$

$$w \frac{dY_i}{dx} = \dot{\Omega}_i \tag{69}$$

Equations 66-69 can also be expressed in terms of the sonic parameter,

$$\eta = 1 - M^2, \tag{70}$$

as

$$\frac{d\rho}{dx} = -\frac{\rho}{w} \frac{\dot{\sigma}}{\eta} \tag{71}$$

$$\frac{dw}{dx} = \frac{\dot{\sigma}}{\eta} \tag{72}$$

$$\frac{dP}{dx} = -\rho w \frac{\dot{\sigma}}{\eta} \tag{73}$$

$$w \frac{dY_i}{dx} = \dot{\Omega}_i. \tag{74}$$

In the Lagrangian description, these equations are

$$\begin{aligned}
\left. \frac{d\rho}{dt} \right|_{X_p} &= -\rho \frac{\dot{\sigma}}{\eta} \\
\left. \frac{dw}{dt} \right|_{X_p} &= w \frac{\dot{\sigma}}{\eta} \\
\left. \frac{dP}{dt} \right|_{X_p} &= -\rho w^2 \frac{\dot{\sigma}}{\eta} \\
\left. \frac{dY_i}{dt} \right|_{X_p} &= \dot{\Omega}_i.
\end{aligned} \tag{75}$$

For either differential system of equations (Eqs. 71-74 or Eq. 75), we can use,

$$\frac{dt}{dX_p} = \frac{1}{w} \quad \text{or} \quad \frac{dX_p}{dt} = w \quad (76)$$

to find the particle path.

It is also interesting to derive an expression for the temperature evolution. To do this, we start with the ideal gas P - v - T equation.

$$P = \rho RT \quad (77)$$

We find the temperature derivative by taking the logarithmic derivative of this equation

$$\frac{dP}{P} = \frac{d\rho}{\rho} + \frac{dR}{R} + \frac{dT}{T} \quad (78)$$

The definition of the gas-specific gas constant,

$$R = \frac{\mathcal{R}}{\overline{W}} = \mathcal{R} \sum_{i=1}^{N_Y} Y_i/W_i, \quad (79)$$

its derivative,

$$\frac{dR}{R} = \sum_{i=1}^{N_Y} \frac{\overline{W}}{W_i} dY_i, \quad (80)$$

and the ZND equations (Eqs. 71-74) lead to

$$\frac{dT}{dx} = \frac{T}{w} \left[(1 - \gamma M^2) \frac{\dot{\sigma}}{\eta} - \sum_{i=1}^{N_Y} \frac{\overline{W}}{W_i} \dot{\Omega}_i \right] \quad (81)$$

or

$$\left. \frac{dT}{dt} \right|_{X_p} = T \left[(1 - \gamma M^2) \frac{\dot{\sigma}}{\eta} - \sum_{i=1}^{N_Y} \frac{\overline{W}}{W_i} \dot{\Omega}_i \right] \quad (82)$$

In these expressions \mathcal{R} is the universal gas constant, \overline{W} is the average molecular weight, and W_i is the weight of species i .

4.2.3 Length Scales

In the ZND detonation model, there are two main length scales: the induction length Δ_i and the energy pulse width Δ_e . We determine these scales from the thermicity profile. Figure 5 indicates that Δ_i is the distance to the maximum thermicity and Δ_e is the half-height width of the thermicity pulse.

4.2.4 Particle Paths

The particle paths shown in Fig. 4 were computed based on the ZND structure of a CJ detonation in stoichiometric hydrogen-air initially at 300 K and 1 bar. In the wave-fixed frame (Fig. 4c), the equations

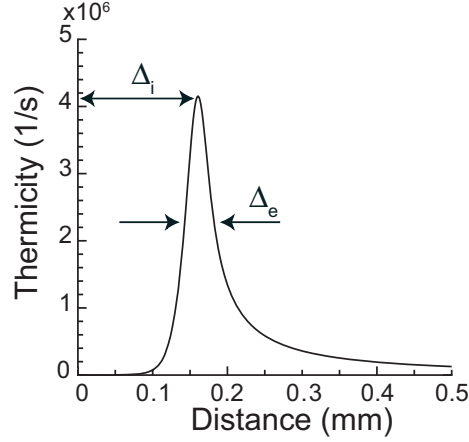


Figure 5: Definition of the induction length Δ_i and energy pulse width Δ_e in terms of the thermicity for a CJ detonation in stoichiometric hydrogen-air initially at 300 K and 1 atm. In this case $\Delta_i = 161 \mu\text{m}$ and $\Delta_e = 43 \mu\text{m}$.

are

$$x_S = 0 \quad (83)$$

$$x_{\Delta_i} = \Delta_i \quad (84)$$

$$x_{\pm\Delta_e/2} = \Delta_i \pm \frac{\Delta_e}{2} \quad (85)$$

$$x_M = \Delta_M \quad (86)$$

$$X_p = \int_{t_S}^t w dt \quad (87)$$

where x_S is the location of the shock (black line), x_{Δ_i} is the end of the induction zone or the location of the thermicity peak (red line), $x_{\pm\Delta_e/2}$ bound the energy release zone (blue lines), x_M is the location of $M = 0.73$ (black dashed line), and X_p is the particle path (green curve). For Figs. 4a and b, we must transform to the lab frame. In these figures, the equations for the lines become

$$x_S^L = U_S t \quad (88)$$

$$x_{\Delta_i}^L = U_S t - \Delta_i \quad (89)$$

$$x_{\pm\Delta_e/2}^L = U_S t - \left(\Delta_i \pm \frac{\Delta_e}{2} \right) \quad (90)$$

$$x_M^L = U_S t - \Delta_M \quad (91)$$

$$X_p^L = \begin{cases} X_p^L(t=0) & t < t_S \\ X_p^L(t=0) + \int_{t_S}^t (U - w) dt & t \geq t_S \end{cases} \quad (92)$$

where t_S is the time when the shock reaches a particle that was originally at $X_P(t=0)$.

Special care must be taken when generating these curves from the discrete data returned from our implementation. The curves in the wave-fixed frame come directly from the discrete data. The distance column corresponds to $X_p = \int w dt$. On the other hand, in the lab frame, creating the discrete particle path array is slightly more challenging. Our implementation uses a variable step size integrator, and

therefore the integrator takes smaller steps within the reaction zone than close to equilibrium. The time array that is returned represents that time elapsed since the shock and particle path intersect. For this reason, “ t ” in the lab frame particle path equation corresponds to t_S plus the time array starting with the first element to assure that the step size remains the same through the reaction zone for all particle paths.

4.3 Eigenvalue Detonation

If η actually vanishes before $\dot{\sigma}$ does, then the solutions for P and ρ will develop singularities and will have to be discarded as nonphysical. This is how the weak solution branch of the detonation adiabat (see Browne et al., 2007) can be ruled out. In order to reach a weak solution, which is supersonic $\eta < 0$, from a subsonic post-shock state, η will have to pass through zero. Unless $\dot{\sigma}$ vanishes exactly at the point $\eta = 0$, no acceptable solution to the structure equations will exist. This implies that $\dot{\sigma}$ must change sign within the reaction zone exactly at the point where η vanishes. This is termed an *eigenvalue* or *pathological* detonation (Fickett and Davis, 1979).

Physically, eigenvalue solutions can occur if competing exothermic and endothermic reactions (Zel’dovich, 1940) or a decrement in the mole number ($\Delta n < 0$) (von Neumann, 1942) cause $\dot{\sigma}$ to change sign within the reaction zone. Computations described subsequently indicate that realistic reaction mechanisms do tend to predict a weak eigenvalue effect in most fuel-oxidizer systems but it is not clear that this can be experimentally observed. Supersonic states are observed (Edwards et al. ; ?; Duff et al. 1958) behind propagating detonations, but this is related to the presence of the instability waves on the detonation front and boundary layers in ducts rather than eigenvalue-type solutions. The variation from the computed CJ velocity is small and there are a number of complicating factors in interpreting the experiments in terms of idealized one-dimensional models based on reaction mechanisms and thermochemical data that have appreciate uncertainties.

Eigenvalue-type solutions are plausible and have been studied in the context of curved detonation waves and frictional flows. Curvature and gradients in the flow behind the detonation wave can compete with the energy release as discussed in the previous section on the shock change equation. Critical wave speeds and curvatures result from an eigenvalue analysis. If the flow is considered quasi-one dimensional, friction at the walls of the duct will compete with the reaction to produce an eigenvalue situation. Models of detonation failure in narrow channels or ducts have been developed around this idea. REFERENCES

What happens at the end of the reaction zone, $x \rightarrow \infty$? For a CJ detonation, the solution of the structure equations should approach the CJ state as $x \rightarrow \infty$. As long as $\dot{\sigma}$ approaches zero faster than η does, the solutions will be well behaved and nonsingular. In practice, there is usually no difficulty because the Mach number used to define η is based on the frozen sound speed a_f and the fluid velocity at the end of a CJ reaction zone approaches the equilibrium sound speed, a_e . The value of the frozen sound speed is always between 1 and 10% larger than the equilibrium value at the end of the reaction zone (Fickett and Davis, 1979), so that η never reaches zero. For overdriven waves, the flow always terminates at a subsonic velocity on the detonation adiabat so there is no difficulty with that case either.

4.4 Numerical Methods

This algorithm solves the ZND detonation governing equations to determine the evolution of the thermodynamic state and the induction time. Our implementation returns the two length scales of interest (see Section 4.2.3), the induction length Δ_i and the energy pulse width Δ_e . By integrating the particle path (Eq. 76), we also return the corresponding induction time τ_i and energy pulse time τ_e .

4.4.1 Initial Conditions

The initial conditions for the simulation are that of a shocked gas mixture. The user must specify the pre-shock initial conditions and either the desired shock speed or the option to use the Chapman-Jouguet detonation speed for the given mixture.

ADD MACH NUMBER CHECK

4.4.2 Algorithm

1. Define known quantities: Upstream State (P_1, T_1, \bar{Y}_1), \bar{W} , \mathcal{R} , error tolerances
2. Seek unknown quantities: Evolution of thermodynamic properties and species ($P(t), T(t), \bar{Y}(t)$) and Induction Time
3. Call program `PostShock` (Browne et al., 2007) to determine the initial conditions for the ZND detonation simulation
 - The `znd.shk` option implements `PostShock_fr` and requires the user to specify the shock speed.
 - The `znd.CJ` option implements `PostShock_fr` and assumes that the shock speed will be the CJ speed.
4. Call a stiff ODE solver (`ode15s` in Matlab, `CVODE` in c++) to iteratively solve Eqs. 71-74 and Eq. 76 subject to the equation of state (Eq. 2) and the definitions of thermicity (Eqs. 42 and 45) and the sonic parameter (Eq. 70).
5. Create an array of the thermicity according to Eqs. 42 and 45.
6. Find the induction length Δ_i , induction time τ_i , exothermic pulse width Δ_e , and exothermic pulse time τ_e in terms of the thermicity.
7. Return $\Delta_i, \tau_i, \Delta_e, \tau_e$, and arrays for $P(t), T(t)$, and $\bar{Y}(t)$

Figure 6 shows the agreement of our new implementation with the legacy Fortran version which uses the CHEMKIN thermodynamic library.

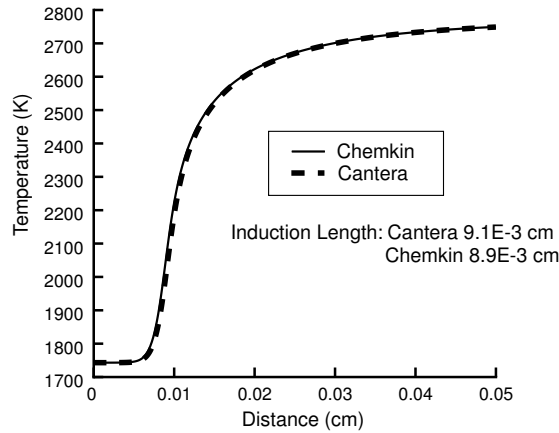


Figure 6: ZND detonation temperature profile simulated by our implementation superimposed over ZND detonation temperature profile simulated by Shepherd’s ZND program. The case is hydrogen air with an equivalence ratio of 0.5, an initial temperature of 300 K, an initial pressure of 1 atm, and a shock speed of 2000 m/s.

4.5 Examples

Here will illustrate the results for a CJ detonation and an overdriven detonation. There is no solution for an underdriven detonation (see Browne et al. (2007) for a detailed explanation). See the following examples:

Matlab: [demo_ZNDCJ.m](#) and [demo_ZNDshk.m](#)

C++: [ZND_Basic](#)

Python/C++: [znd.py](#)

4.5.1 CJ Detonation

The Chapman-Jouguet detonation velocity is the minimum wave speed that admits a solution. The CJ case is depicted in the P - v plane in Fig. 3. We see that the Rayleigh line is tangent to the product Hugoniot. The spatial profiles for pressure, temperature, density, velocity, and species for a CJ detonation in an initially stoichiometric mixture of hydrogen and air at 300 K and 1 atm is shown in Figs. 7 and 8. We used the Matlab demonstration [demo_ZNDCJ.m](#) to generate these results. The thermicity profile for this case is superposed on the temperature profile and shown in Figure 9.

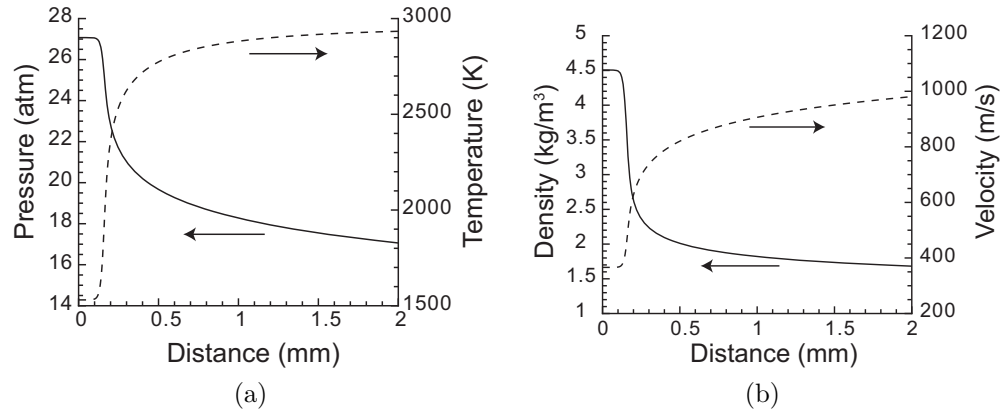


Figure 7: ZND structure for a CJ detonation stoichiometric hydrogen-air initially at 300 K and 1 atm. (a) temperature and pressure profiles, (b) density and velocity profiles

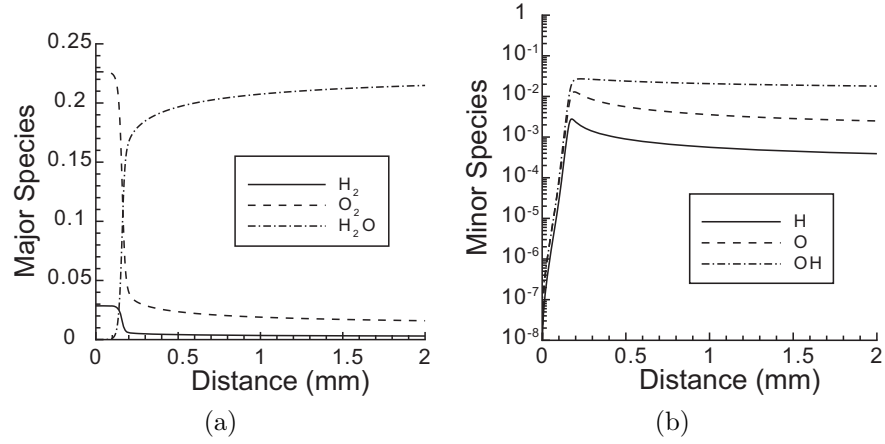


Figure 8: ZND structure for a CJ detonation stoichiometric hydrogen-air initially at 300 K and 1 atm. (a) major species profiles, (b) minor species profiles

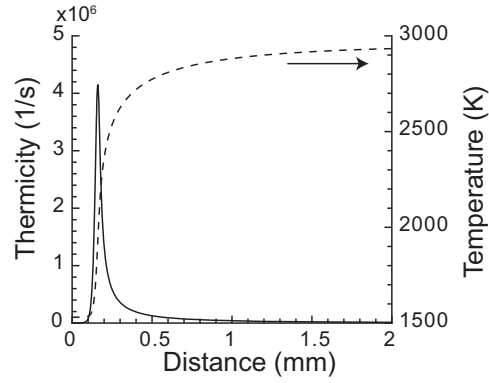


Figure 9: Thermicity ($\dot{\sigma}$) and temperature ZND structure for a CJ detonation in stoichiometric hydrogen-air initially at 300 K and 1 atm.

4.5.2 Overdriven Detonation

If we increase the speed of the front shock, the Rayleigh line becomes steeper. This is shown in Fig. 10 for $U = 1.1U_{CJ}$. Unless we have an eigenvalue detonation (see Section 4.3), only the upper intersection,

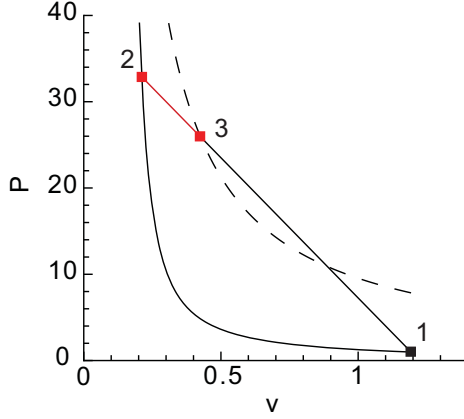


Figure 10: Path (red) between frozen Hugoniot (solid) and equilibrium Hugoniot (dashed) for a ZND detonation traveling at $U = 1.1U_{CJ}$.

the strong solution, is admissible. The spatial profiles for pressure, temperature, density, velocity, and species for an overdriven detonation ($U = 1.1U_{CJ}$) in an initially stoichiometric mixture of hydrogen and air at 300 K and 1 atm is shown in Figs. 7 and 8. We used the Matlab demonstration [demo_ZNDshk.m](#) to generate these results. The thermicity profile for this case is superposed on the temperature profile and shown in Fig. 13.

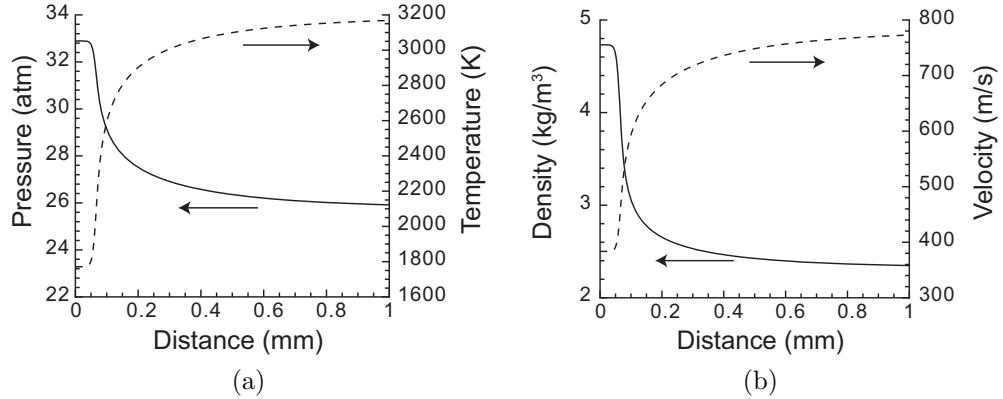


Figure 11: ZND structure for an overdriven detonation ($U = 1.1U_{CJ}$) stoichiometric hydrogen-air initially at 300 K and 1 atm. (a) temperature and pressure profiles, (b) density and velocity profiles

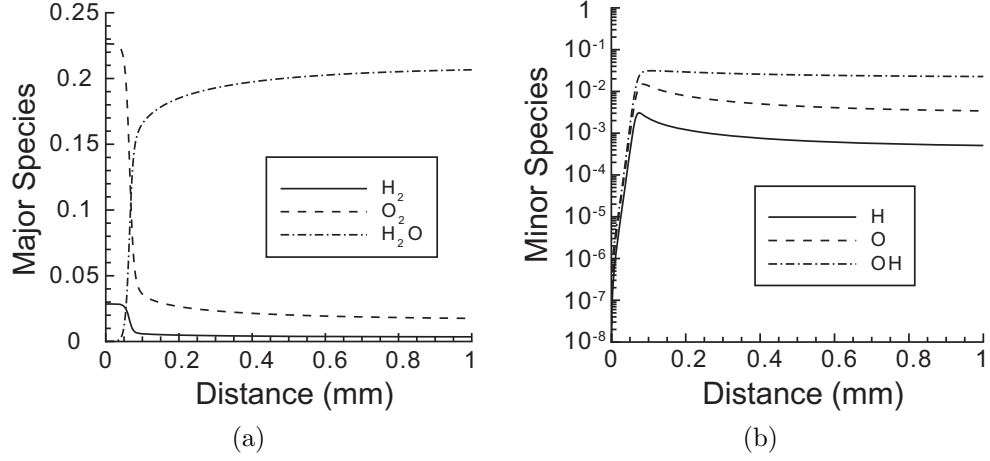


Figure 12: ZND structure for an overdriven detonation ($U = 1.1U_{CJ}$) stoichiometric hydrogen-air initially at 300 K and 1 atm. (a) major species profiles, (b) minor species profiles

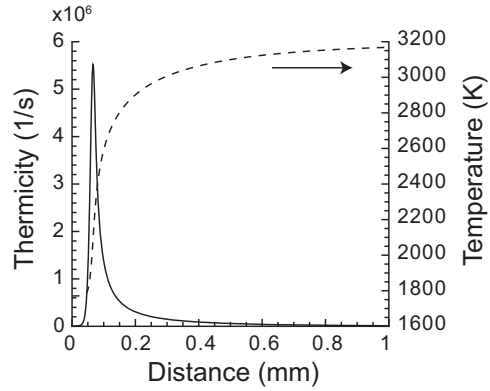


Figure 13: Thermicity ($\dot{\sigma}$) and temperature ZND structure for an overdriven detonation ($U = 1.1U_{CJ}$) stoichiometric hydrogen-air initially at 300 K and 1 atm.

5 Extensions to the ZND model

Three useful extensions to the ZND model equations have been developed. [Eckett et al. \(2000\)](#) derived the model in the case of a unsteady curved front shock. [Klein et al. \(1995\)](#) describes a subset of this unsteady model which focuses specifically on curved waves. CITE MCGILL give a model that includes frictional effects.

5.1 Unsteady Model

[Eckett et al. \(2000\)](#) derives an extension of the ZND model by including geometry and unsteadiness in the leading shock. The reactive Euler equations for the most general case are

$$\begin{aligned}\frac{D\rho}{Dt^L} + \rho \frac{\partial u}{\partial x^L} + \frac{j}{x^L} \rho u &= 0 \\ \frac{Du}{Dt^L} + \frac{1}{\rho} \frac{\partial P}{\partial r^L} &= 0 \\ \frac{DP}{Dt^L} - a_f^2 \frac{D\rho}{Dt^L} &= \rho a_f^2 \dot{\sigma} \\ \frac{DY_i}{Dt^L} &= \dot{\Omega}_i\end{aligned}\tag{93}$$

where j is the dimensionality, i.e. $j = 0$ for a planar shock, $j = 1$ for a cylindrical shock, or $j = 2$ for a spherical shock. If we assume that the shock speed U is only a function of time, these can be rewritten in the wave-fixed frame in terms of $\dot{\sigma}$ and η .

$$\begin{aligned}\eta \frac{D\rho}{Dt} &= -\rho \dot{\sigma} + \frac{j}{X_S - x} \rho M^2 (U - w) + \frac{\rho w}{a_f^2} \frac{dU}{dt} - \frac{\rho w}{a_f^2} \frac{\partial w}{\partial t} + \frac{1}{a_f^2} \frac{\partial P}{\partial t} \\ \eta \frac{Dw}{Dt} &= w \dot{\sigma} - \frac{j}{X_S - x} w (U - w) - M^2 \frac{dU}{dt} + \frac{\partial w}{\partial t} - \frac{w}{\rho a_f^2} \frac{\partial P}{\partial t} \\ \eta \frac{DP}{Dt} &= -\rho w^2 \dot{\sigma} + \frac{j}{X_S - x} \rho w^2 (U - w) + \rho w \frac{dU}{dt} - \rho w \frac{\partial w}{\partial t} + \frac{\partial P}{\partial t} \\ \frac{DY_i}{Dt} &= \dot{\Omega}_i\end{aligned}\tag{94}$$

where X_S is the location of the shock. The rate of change of temperature for this model is

$$\begin{aligned}\eta c_P \frac{DT}{Dt} &= -(1 - \gamma M^2) \sum e_i \dot{\Omega}_i - \frac{a_f^2}{\gamma} \sum \frac{\bar{W}}{W_i} \dot{\Omega}_i \\ &\quad + \frac{j}{X_S - x} w^2 (U - w) + w \frac{dU}{dt} - w \frac{\partial w}{\partial t} + \frac{1}{\rho} \frac{\partial P}{\partial t}\end{aligned}\tag{95}$$

If the shock is planar and the detonation is steady, these equations reduce to the ZND equations (Eqs. 71-74) presented in Section 4.

5.2 Steady Curved Wave Model

[Klein et al. \(1995\)](#) present an extension of the ZND model that allows for curvature only of the front wave. They define a normalized stream tube area change ([Bdzil and Stewart, 1988](#))

$$\alpha = \frac{1}{A} \frac{dA}{dx} = \frac{j}{X_S} \left(\frac{U}{w} - 1 \right)\tag{96}$$

Again j is the dimensionality and X_S is the location of the shock. In terms of α , the extension of the ZND model is

$$\begin{aligned}\frac{d\rho}{dx} &= -\frac{\rho}{w} \frac{(\dot{\sigma} - wM^2\alpha)}{\eta} \\ \frac{dw}{dx} &= \frac{(\dot{\sigma} - w\alpha)}{\eta} \\ \frac{dP}{dx} &= -\rho w \frac{(\dot{\sigma} - w\alpha)}{\eta} \\ \frac{dY_i}{dx} &= \frac{\dot{\Omega}_i}{w}\end{aligned}\tag{97}$$

In the case of a planar shock, these reduce to the ZND equations (Eqs. 71-74) presented in Section 4.

5.3 Steady Detonation with Friction

ADD SECTION

6 Constant Volume Explosion Model

In this section, we will present the constant volume explosion model which is a limiting case of the ZND model (see Section 4). We will first give a graphical interpretation and present the mathematical model. Then we will describe our algorithm, and finally give an example.

6.1 Physical Model

The ZND model (Section 4) involves both chemical reaction and fluid dynamics. A simpler model could monitor a small constant volume packet of reacting gas. As described in Section 3, tracking the time evolution of a fluid packet is the Lagrangian description of the field. If the specific volume is held constant, the Rayleigh line between the reactant and product Hugoniot curves is vertical as shown in Figure 14 which implies infinitely fast combustion ($w \rightarrow \infty$).

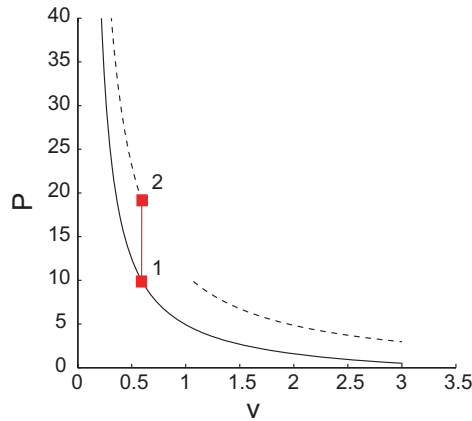


Figure 14: Path (blue) between frozen Hugoniot (solid) and equilibrium Hugoniot (dashed) for a constant volume explosion.

6.2 Mathematical Model

Like the ZND model (Section 4), the constant volume explosion model can be expressed as a differential species conservation equation subject to algebraic physical constraints or as a purely differential system of equations.

6.2.1 Algebraic Differential System

The algebraic-differential system of equations corresponds to the Lagrangian conservation of species equation

$$\left. \frac{dY_i}{dt} \right|_{X_p} = \dot{\Omega}_i, \quad (98)$$

where X_p is the particle path, and an algebraic constraint determined by the shock jump conditions (Eq. 15). The simplest way to specify this algebraic constraint is to examine the following form of the Hugoniot curve equation

$$\Delta e = \Delta v \frac{P_1 + P_2}{2}. \quad (99)$$

We see that if the volume is constant then,

$$\Delta e = 0 \quad (100)$$

which is appropriate because in a rigid isolated system, energy is conserved. In the case of a perfect gas ($\gamma = \text{constant}$) with a single progress variable, we can use

$$e(T) = \frac{1}{\gamma - 1} \frac{P}{\rho} - \lambda q \quad (101)$$

to specify P in terms of species.

$$P = (\gamma - 1) \frac{e(T) + \lambda q}{\rho} \quad (102)$$

6.2.2 Differential System

The constant volume explosion model is a Lagrangian model and therefore appears to be an unsteady zero-dimensional system of equations. For this model, we recall the definition of η (Eq. 70) and look at the limiting behavior of Eq. 75 as the velocity goes to infinity. The limiting equations are

$$\left. \frac{d\rho}{dt} \right|_{X_p} = 0 \quad (103)$$

$$\left. \frac{dw}{dt} \right|_{X_p} = 0 \quad (104)$$

$$\left. \frac{dP}{dt} \right|_{X_p} = -\rho a_f^2 \dot{\sigma} \quad (105)$$

$$\left. \frac{dY_i}{dt} \right|_{X_p} = \dot{\Omega}_i. \quad (106)$$

We find that as expected the density (or specific volume) remains constant and the pressure varies. We could also use the constant volume limit of Eq. 26.

$$\left. \frac{de}{dt} \right|_{X_p} = 0 \quad (107)$$

This corresponds more directly to Eq. 100. Most commonly, we compute the temperature as a function of time. The temperature equation can be derived from either energy equation (Eq. 105 or Eq. 107) or as the limit of the ZND temperature evolution equation (Eq. 82).

$$\left. \frac{dT}{dt} \right|_{X_p} = -\frac{1}{c_v} \sum_{i=1}^{N_Y} e_i \dot{\Omega}_i \quad (108)$$

A more detailed derivation of Eq. 108 is given in Appendix A

6.2.3 Time Scales

In the CV detonation model, there is one main time scale: the induction time τ_i . We determine this scale from the temperature gradient profile. Figure 15 indicates that τ_i is the time to the maximum temperature gradient.

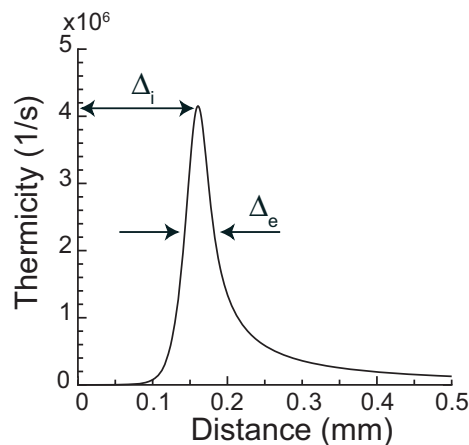


Figure 15: Definition of the induction time τ_i in terms of the temperature gradient for a constant volume explosion in stoichiometric hydrogen-air initially at the von Neumann point. In this case $\tau_i = 161 \mu\text{s}$.

6.3 Numerical Method

The algorithm below solves the constant volume explosion governing equations (Eqs. 98 and 108) to determine the evolution of the thermodynamic state and the induction time. Our algorithm returns three different interpretations of the induction time, each dependent on the maximum temperature gradient. We look for the time when the temperature gradient is maximum, the time when the temperature gradient has reached 90% of its maximum, and the time when the temperature gradient has reached 10% of its maximum.

6.3.1 Initial Conditions

The initial conditions for this model consist of a mixture of reactants at high temperature and pressure. The user can either specify the initial pressure and temperature desired or use the frozen post-shock

state calculator (Browne et al., 2007). In both demos included with the toolbox, the initial conditions are determined by shocking a mixture at standard temperature and pressure. In these cases, the user must specify the pre-shock initial conditions and either the desired shock speed or the option to use the Chapman-Jouguet detonation speed for the given mixture.

6.3.2 Algorithm

1. Define Known quantities: Upstream State (P_1, T_1, \bar{Y}_1), \bar{W} , \mathcal{R} , error tolerances
2. Seek Unknown quantities: Evolution of thermodynamic properties and species ($P(t), T(t), \bar{Y}(t)$) and induction time
3. Specify the initial state. To elevate the temperature and pressure by shocking the initial mixture, call program `PostShock_fr` (Browne et al., 2007). Both demos below begin with a shocked mixture.
 - `cv_shk` option implements `PostShock_fr` and requires the user to specify the shock speed.
 - The `cv_CJ` option implements `PostShock_fr` and assumes that the shock speed will be the CJ speed.
4. Call a stiff ODE solver (`ode15s` in Matlab, `CVODE` in c++) to iteratively solve Eqs. 98 and 108 subject to the equation of state (Eq. 2).
5. Create an array of the temperature gradient according to Eq. 108.
6. Find the three interpretations of the induction time
 - Coordinate of maximum temperature gradient
 - Coordinate when temperature gradient reaches 10% of its maximum
 - Coordinate when temperature gradient reaches 90% of its maximum
7. Return three values of the induction time and arrays for $P(t)$, $T(t)$, and $\bar{Y}(t)$

Figure 16 shows the agreement of our new implementation with the legacy Fortran version which uses the CHEMKIN thermodynamic library.

6.4 Example

Here will illustrate the results for a constant volume explosion starting from the von Neumann point. The von Neumann state is the frozen post-shock state behind a shock traveling at the CJ detonation velocity for the given mixture. See the following examples:

Matlab: `demo.cvCJ.m` and `demo.cvshk.m`

Python: `demo.cvCJ.py` and `demo.cvshk.py`

- CV basic
- Discuss Westbrook and Urtiew

The spatial profiles for pressure, temperature, density, velocity, and species for a constant volume explosion in a stoichiometric mixture of hydrogen and air initially at the von Neumann point (state 2 in Fig. 3) is shown in Figs. 17 and 18. We used the Matlab demonstration `demo.cvCJ.m` to generate these results. We calculate the induction time as the time corresponding to the maximum temperature gradient. The temperature gradient profile for this case is superposed on the temperature profile and shown in Fig. 19.

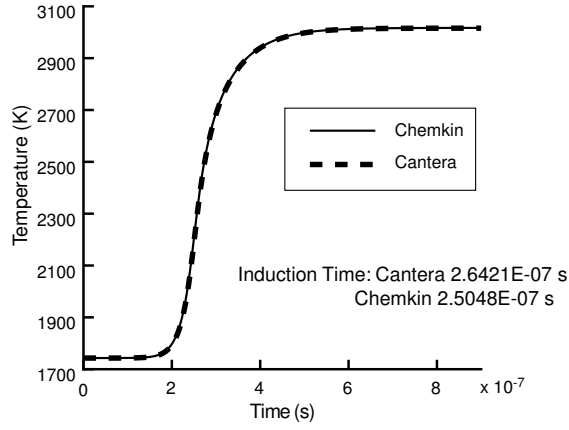


Figure 16: Control volume explosion simulated by PostShock_fr superimposed over control volume explosion simulated by Shepherd's CV program. The case is hydrogen air with an equivalence ratio of 0.5, an initial temperature of 300 K, an initial pressure of 1 atm, and a shock speed of 2000 m/s.

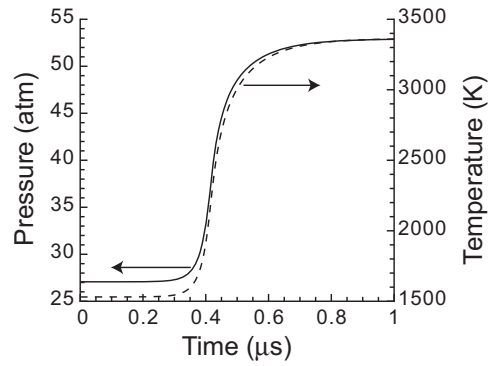


Figure 17: CV structure for a stoichiometric mixture of hydrogen-air initially at the von Neumann point. (a) temperature and pressure profiles, (b) density and velocity profiles

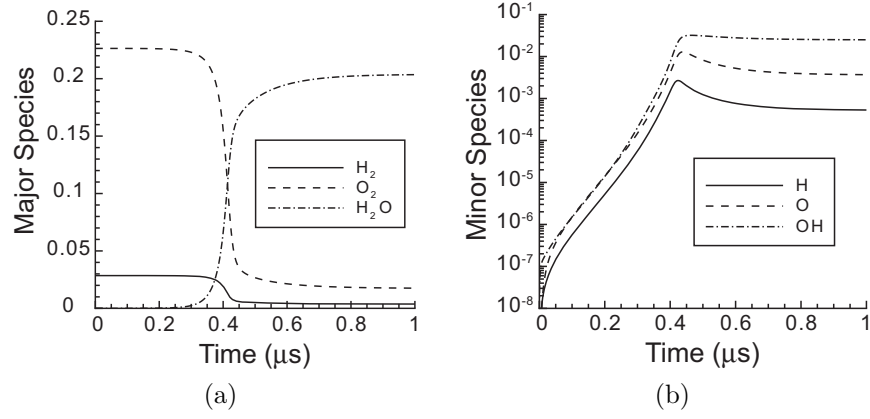


Figure 18: CV structure for a stoichiometric mixture of hydrogen-air initially at the von Neumann point. (a) major species profiles, (b) minor species profiles

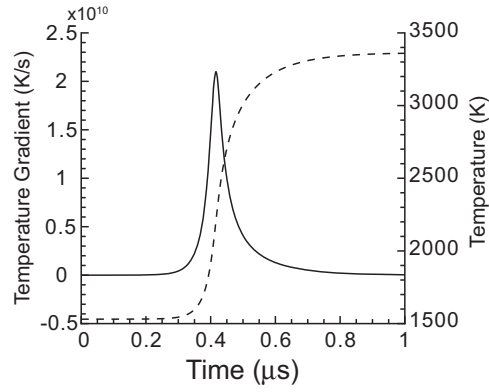


Figure 19: Temperature gradient and temperature CV structure for a stoichiometric mixture of hydrogen-air initially at the von Neumann point.

7 Constant Pressure Explosion Model

In this section, we will present the constant pressure explosion model which is a limiting case of the ZND model (see Section 4). We will first give a graphical interpretation and present the mathematical model. Then we will describe our algorithm, and finally give an example.

7.1 Physical Model

A second model which simplifies the ZND equations could monitor a small constant pressure packet of reacting gas. As described in Section 3, tracking the time evolution of a fluid packet is the Lagrangian description of the field. If the pressure is held constant, the Rayleigh line between the reactant and product Hugoniot curves is horizontal as shown in Figure 14 which implies infinitely slow combustion ($w \rightarrow \infty$).

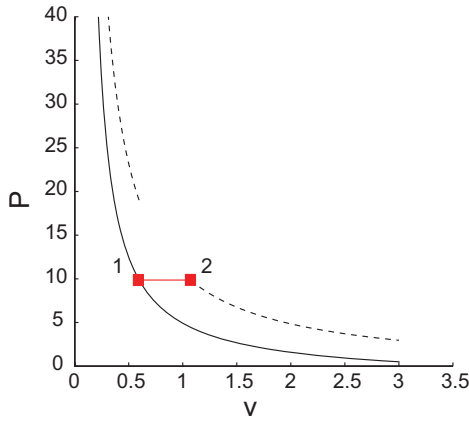


Figure 20: Path (red) between frozen Hugoniot (solid) and equilibrium Hugoniot (dashed) for a constant pressure explosion.

7.2 Mathematical Model

Like the ZND model (Section 4), the constant pressure explosion model can be expressed as a differential species conservation equation subject to algebraic physical constraints or as a purely differential system of equations.

7.2.1 Algebraic Differential System

The algebraic-differential system of equations corresponds to the Lagrangian conservation of species equation

$$\left. \frac{dY_i}{dt} \right|_{X_p} = \dot{\Omega}_i, \quad (109)$$

where X_p is the particle path, and an algebraic constraint determined by the shock jump conditions (Eq. 15). The simplest way to specify this algebraic constraint is to examine the following form of the Hugoniot curve equation

$$\Delta h = \Delta P \frac{v_1 + v_2}{2}. \quad (110)$$

We see that if the pressure is constant then,

$$\Delta h = 0 \quad (111)$$

which is appropriate because in a constant pressure system, enthalpy is conserved. In the case of a perfect gas ($\gamma = \text{constant}$) with a single progress variable, we can use

$$h(T) = \frac{\gamma}{\gamma - 1} \frac{P}{\rho} - \lambda q \quad (112)$$

to specify ρ in terms of species.

$$\rho = (\gamma - 1) \frac{h(T) + \lambda q}{P} \quad (113)$$

7.2.2 Differential System

The constant pressure explosion model is a Lagrangian model and therefore appears to be an unsteady zero-dimensional system of equations. For this model, we recall the definition of η (Eq. 70) and look at the limiting behavior of Eq. 75 as the velocity goes to zero. The limiting equations are

$$\left. \frac{d\rho}{dt} \right|_{X_p} = -\rho\dot{\sigma} \quad (114)$$

$$\left. \frac{dw}{dt} \right|_{X_p} = 0 \quad (115)$$

$$\left. \frac{dP}{dt} \right|_{X_p} = 0 \quad (116)$$

$$\left. \frac{dY_i}{dt} \right|_{X_p} = \dot{\Omega}_i. \quad (117)$$

We find that as expected the pressure remains constant and the density varies. We could also use the constant pressure limit of Eq. 27.

$$\left. \frac{dh}{dt} \right|_{X_p} = 0 \quad (118)$$

This corresponds more directly to Eq. 111. As in the constant volume model, we commonly compute the temperature as a function of time. The temperature equation can be derived from either energy equation (Eq. 116 or Eq. 118) or as the limit of the ZND temperature evolution equation (Eq. 82).

$$\left. \frac{dT}{dt} \right|_{X_p} = -\frac{1}{c_P} \sum_{i=1}^{N_Y} h_i \dot{\Omega}_i \quad (119)$$

A more detailed derivation of Eq. 119 is given in Appendix A

7.3 Numerical Method

7.4 Example

8 Applications

- Compare and contrast scales from ZND and CV

- Activation Energy
- τ, Δ vs $\phi, U/U_{CJ}, P_1$
- cell size correlations
- critical tube diameter

In this section we will present some useful applications for these programs. First in Section 8.1, we will compare the time scales computed with the ZND model and with those computed with the constant volume explosion model. As discussed in Section 6, the constant volume explosion model is often used as an approximation for the ZND model. We can also use these models to approximate the effective activation energy. A methodology for this is presented in Section 8.2. Section 8.3 uses these models to determine how the length and time scales vary with equivalence ratio, overdrive (U/U_{CJ}), and initial pressure. Finally, Section 8.4 gives some correlation expressions between the length and time scales and the dynamic detonation parameters (Lee, 1984).

8.1 Time Scale Comparison

8.2 Effective Activation Energy

8.3 Variance with Initial Conditions

8.4 Dynamic Detonation Parameters

9 Summary

ADD SECTION

References

- J. B. Bdzil and D. S. Stewart. Modeling of two-dimensional detonations with detonation shock dynamics. *Phys. Fluids*, 1261, 1988. [31](#)
- S. Browne, J. Ziegler, and J. E. Shepherd. Numerical solution methods for shock and detonation jump conditions. Technical Report FM2006.007, GALCIT, 2007. [2](#), [6](#), [10](#), [12](#), [18](#), [19](#), [21](#), [25](#), [26](#), [27](#), [35](#)
- W. Doering. On detonation processes in gases. *Ann. Phys.*, 43:421–436, 1943. [19](#)
- C. A. Eckett. *Numerical and analytical studies of the dynamics of gaseous detonations*. PhD thesis, California Institute of Technology, Pasadena, California, September 2000. [11](#)
- C. A. Eckett, J. J. Quirk, and J. E. Shepherd. The role of unsteadiness in direct initiation of gaseous detonations. *J. Fluid Mech.*, 421:147–183, 2000. [31](#)
- W. Fickett and W. Davis. *Detonation Theory and Experiment*. Dover Publications, INC., 1979. [14](#), [25](#)
- D. Goodwin. Cantera: object-oriented software for reacting flows. Technical report, California Institute of Technology, 2005. <http://www.cantera.org>. [9](#)
- B. F. Gray and C. H. Yang. On the unification of the thermal and chain theories of explosion limits. *J. Phys. Chem.*, 69(8):2747–2750, 1965. [11](#)
- R. J. Kee, F. M. Rupley, and J. A. Miller. The CHEMKIN thermodynamic data base. Technical Report SAND87-8215, Sandia National Laboratories, 1987. [9](#)
- R. Klein, J. C. Krok, and J. E. Shepherd. Curved quasi-steady detonations: asymptotic analysis and detailed chemical kinetics. Technical Report FM95-04, California Institute of Technology, 1995. [31](#)
- V. P. Korobeinikov, V. A. Levin, V. V. Markov, and G. G. Cher. Propagation of blast wave in combustible gas. *Astronautica Acta*, 17:529–537, 1972. [11](#)
- J. H. Lee. Dynamic parameters of gaseous detonations. *Ann. Rev. Fluid Mech.*, 16:311–336, 1984. [40](#)
- M. H. Lefebvre, E. S. Oran, and K. Kailasanath. Computations of detonation structure: The influence of model parameters. Technical Report NRL Memorandum Report NRL/MR/4404-92-6961, Naval Research Laboratory, 1992. [12](#)
- U. Maas and S. B. Pope. Simplifying chemical kinetics: Intrinsic low-dimensional manifolds in composition space. *Combust. Flame*, 88:239–264, 1992. [11](#)
- E. S. Oran, J. P. Boris, T. Young, M. Flanigan, T. Burks, and M. Picone. Numerical simulations of detonations in hydrogen-air and methane-air mixtures. In *18th Symp. (Intl) on Combustion*, pages 1641–1649, 1981. [11](#)
- N. Peters. Systematic reduction of flame kinetics: Principles and details. *Prog. Astronaut. Aeronaut.*, 113:67–86, 1988. [11](#)
- N. N. Semenov. *Chemical Kinetics and Chain Reactions*. Clarendon Press, Oxford, 1935. [11](#)
- J. E. Shepherd. Chemical kinetics of hydrogen-air-diluent detonations. *Prog. Astronaut. Aeronaut.*, 106:263–293, 1986. [9](#)
- G. P. Smith, D. M. Golden, M. Frenklach, N. W. Moriarty, B. Eiteneer, M. Goldenberg, C. T. Bowman, R. K. Hanson, S. Song, W. C. Gardiner, V. V. Lissianski Jr., and Z. Qin. GRI-Mechanism 3.0. http://www.me.berkeley.edu/gri_mech, 1999. [8](#), [9](#), [11](#)

- A. S. Tomlin, T. Turanyi, and M. J. Pilling. Mathematical tools for the construction, investigation, and reduction of combustion mechanisms. In M. J. Pilling, editor, *Low-temperature combustion and autoignition*, pages 293–437. Elsevier, 1997. [11](#)
- B. Varatharajan and F. A. Williams. Chemical-kinetic descriptions of high-temperature ignition and detonation of acetylene-oxygen-diluent systems. *Combust. Flame*, 124(4):623–645, 2001. [11](#)
- B. Varatharajan, M. Petrova, F. A. Williams, and V. Tangirala. Two-step chemical-kinetic description for hydrocarbon-oxygen-diluent ignition and detonation applications. In *Proc. Combust. Inst.*, volume 30, pages 1869–1877, 2005. [11](#)
- J. von Neumann. Theory of detonation waves. In A. J. Taub, editor, *John von Neumann, Collected Works*. Macmillan, New York, 1942. [19](#), [25](#)
- Ia. B. Zel’dovich. On the theory of the propagation of detonation in gaseous systems. *Zh. Eksp. Teor. Fiz.*, 10:542–568, 1940. [19](#), [25](#)

A Temperature Derivatives

In order to derive find expressions for the temperature evolution of each model, we start with the ideal gas P - ρ - T relation.

$$P = \rho RT \quad (\text{A.1})$$

This leads to the following logarithmic derivation relationship.

$$\frac{dP}{P} = \frac{d\rho}{\rho} + \frac{dR}{R} + \frac{dT}{T} \quad (\text{A.2})$$

Here R is the gas-specific gas constant,

$$R = \frac{\mathcal{R}}{\overline{W}} = \mathcal{R} \sum_{i=1}^{N_Y} \frac{Y_i}{W_i}. \quad (\text{A.3})$$

The derivative of R is related to the evolution of the species in the following way

$$\frac{dR}{R} = \frac{1}{R} \sum_{i=1}^{N_Y} \frac{\mathcal{R}}{\overline{W}} \frac{\overline{W}}{W_i} dY_i = \sum_{i=1}^{N_Y} \frac{\overline{W}}{W_i} dY_i \quad (\text{A.4})$$

Now the temperature derivative in a steady flow is

$$\frac{dT}{dx} = T \left[\frac{1}{P} \frac{dP}{dx} - \frac{1}{\rho} \frac{d\rho}{dx} - \sum_{i=1}^{N_Y} \frac{\overline{W}}{W_i} \frac{dY_i}{dx} \right], \quad (\text{A.5})$$

and if we insert the thermicity equations (Eqs. 71-74),

$$\frac{dT}{dx} = T \left[-\frac{\rho w}{P} \frac{\dot{\sigma}}{\eta} + \frac{1}{w} \frac{\dot{\sigma}}{\eta} - \sum_{i=1}^{N_Y} \frac{\overline{W}}{W_i} \frac{\dot{\Omega}_i}{w} \right]. \quad (\text{A.6})$$

By grouping terms and recalling the definition of the frozen sound speed $a_f^2 = \gamma P / \rho$, the temperature equation becomes

$$\frac{dT}{dx} = \frac{T}{w} \left[\left(1 - \frac{\gamma w^2}{a_f^2} \right) \frac{\dot{\sigma}}{\eta} - \sum_{i=1}^{N_Y} \frac{\overline{W}}{W_i} \dot{\Omega}_i \right]. \quad (\text{A.7})$$

Finally, the ZND temperature equation is

$$\frac{dT}{dx} = \frac{T}{w} \left[(1 - \gamma M^2) \frac{\dot{\sigma}}{\eta} - \sum_{i=1}^{N_Y} \frac{\overline{W}}{W_i} \dot{\Omega}_i \right] \quad (\text{A.8})$$

or

$$\left. \frac{dT}{dx} \right|_{x_p} = w \frac{dT}{dx} = T \left[(1 - \gamma M^2) \frac{\dot{\sigma}}{\eta} - \sum_{i=1}^{N_Y} \frac{\overline{W}}{W_i} \dot{\Omega}_i \right]. \quad (\text{A.9})$$

A.1 Limiting Behavior

The constant volume explosion is the limit of the ZND equations as velocity goes to infinity $w \rightarrow \infty$. The velocity only appears in the first term and its limit is

$$T \left(1 - \gamma \frac{w^2}{a_f^2}\right) \frac{\dot{\sigma}}{\left(1 - \frac{w^2}{a_f^2}\right)} \rightarrow T\gamma\dot{\sigma}. \quad (\text{A.10})$$

Now we can rearrange the terms as follows to find the correct expression for the constant volume model.

$$\left. \frac{dT}{dx} \right|_{X_p} = T \left[\gamma \sum_{i=1}^{N_Y} \left(\frac{\bar{W}}{W_i} - \frac{h_i}{c_P T} \right) \dot{\Omega}_i - \sum_{i=1}^{N_Y} \frac{\bar{W}}{W_i} \dot{\Omega}_i \right] \quad (\text{A.11})$$

$$= T \sum_{i=1}^{N_Y} \left[(\gamma - 1) \frac{\bar{W}}{W_i} - \frac{\gamma}{c_P} \frac{h_i}{T} \right] \dot{\Omega}_i \quad (\text{A.12})$$

$$= T \sum_{i=1}^{N_Y} \left[(\gamma - 1) \frac{\bar{W}}{W_i} - \frac{e_i + R_i T}{c_v T} \right] \dot{\Omega}_i \quad (\text{A.13})$$

$$= T \sum_{i=1}^{N_Y} \left[(\gamma - 1) \frac{\bar{W}}{W_i} - \frac{e_i + R_i T}{c_v T} \right] \dot{\Omega}_i \quad (\text{A.14})$$

$$= -\frac{1}{c_v} \sum_{i=1}^{N_Y} e_i \dot{\Omega}_i + T \sum_{i=1}^{N_Y} \left[(\gamma - 1) \frac{\bar{W}}{W_i} - \frac{\mathcal{R}}{\bar{W}} \frac{\bar{W}}{W_i} \frac{\gamma - 1}{R} \right] \dot{\Omega}_i \quad (\text{A.15})$$

$$= -\frac{1}{c_v} \sum_{i=1}^{N_Y} e_i \dot{\Omega}_i + T \sum_{i=1}^{N_Y} \left[(\gamma - 1) \frac{\bar{W}}{W_i} - (\gamma - 1) \frac{\bar{W}}{W_i} \right] \dot{\Omega}_i \quad (\text{A.16})$$

$$\left. \frac{dT}{dx} \right|_{X_p} = -\frac{1}{c_v} \sum_{i=1}^{N_Y} e_i \dot{\Omega}_i \quad (\text{A.17})$$

On the other hand, the constant pressure model is the limit as the velocity goes to zero $w \rightarrow 0$. Again, the velocity only appears in the first term and its limit is

$$T \left(1 - \gamma \frac{w^2}{a_f^2}\right) \frac{\dot{\sigma}}{\left(1 - \frac{w^2}{a_f^2}\right)} \rightarrow T\dot{\sigma}. \quad (\text{A.18})$$

Now we can rearrange the terms as follows to find the correct expression for the constant volume model.

$$\left. \frac{dT}{dx} \right|_{X_p} = T \left[\sum_{i=1}^{N_Y} \left(\frac{\bar{W}}{W_i} - \frac{h_i}{c_P T} \right) \dot{\Omega}_i - \sum_{i=1}^{N_Y} \frac{\bar{W}}{W_i} \dot{\Omega}_i \right] \quad (\text{A.19})$$

$$= T \sum_{i=1}^{N_Y} -\frac{h_i}{c_P T} \dot{\Omega}_i \quad (\text{A.20})$$

$$\left. \frac{dT}{dx} \right|_{X_p} = -\frac{1}{c_P} \sum_{i=1}^{N_Y} h_i \dot{\Omega}_i \quad (\text{A.21})$$

B Functions

This section is intended to be a quick reference for learning and usage. Please refer to the [website](#) for installation details.

Below we have provided a brief description of the functions in the Shock and Detonation Toolbox that numerically calculate shock jump conditions. For each function, we give links to the Matlab and Python implementations of these functions.

B.1 Constant Volume Explosion

- **cv_shk**
Inputs Initial Conditions and Returns Plots of Constant Volume Explosion.
Matlab Function - [cv_shk.m](#)
Python Code - cv_shk (in [CV.py](#))
- **cv_CJ**
Inputs Initial Conditions and Returns Plots of Constant Volume Explosion for the CJ Case -
Output File: "fname_Ucj.plt" compatible with Tecplot.
Matlab Function - [cv_CJ.m](#)
Python Code - cv_CJ (in [CV.py](#))
- **explosion**
Constant Volume Explosion, a "zero dimensional" implementation with no length scale.
Matlab Function - [explosion.m](#)
Python Code - explosion (in [CV.py](#))
- **uvsys**
ODE system for a constant-volume, adiabatic reactor. Evaluates the system of ordinary differential equations for an adiabatic, constant-volume, zero-dimensional reactor. It assumes that the 'gas' object represents a reacting ideal gas mixture. Based on `conuv.m` from the Cantera toolbox, this function contains the equations passed to `ode15s` for a constant volume explosion.
Matlab Function - [uvsys.m](#)
Python Code - N/A

B.2 ZND Detonation

B.2.1 Matlab Implementation

See the following Matlab examples:

[demo_ZNDCJ.m](#) and [demo_ZNDshk.m](#)

- **znd_shk**
Inputs Initial Conditions and Returns Plots of ZND Detonation, assumming that the intial gas goes through a shock wave with a frozen (rather than chemically equilibrated) state. Output Files: "fname_U1_znd.plt" & "fname_U1_znd2.plt" compatible with Tecplot.
Matlab Function - [znd_shk.m](#)
- **znd_CJ**
Inputs Initial Conditions and Returns Plots of ZND Detonation for the CJ Case – Output Files: "fname_Ucj_znd.plt" & "fname_Ucj_znd2.plt" compatible with Tecplot.
Matlab Function - [znd_CJ.m](#)
- **znd_detonation**
ZND Model Detonation.
Matlab Function - [znd_detonation.m](#)

- **ZNDReactor**

Contains the set of ODE's to solve ZND Detonation Problem that are passed to `ode15s` for a ZND detonation.

Matlab Function - [ZNDReactor.m](#)

B.2.2 Python/C++ Implementation

Cantera includes a python wrapper for the constant volume explosion model governing equations, but does not provide a wrapper for the ZND equations. We included a wrapper with the python version of the Shock and Detonation toolbox. In order to use this feature, the user must first compile the C++ program ZND. Instructions for doing this can be found on the [C++ ZND Program website](#). Once this program is compiled, the user can run ZND simulations directly with an input file.

If the user would rather use python to create the appropriate input file and/or run the C++ program in a loop, they can use our wrapper. Details for using the wrapper are given on the [Python Wrapper website](#).